Rescattering contributions to the photoproduction of kaons from the deuteron

Oren V. Maxwell
Department of Physics, Florida International University, University Park, Miami, Florida 33199, USA
(Received 1 May 2003; revised manuscript received 12 November 2003; published 15 March 2004)

A model is developed for the reaction $\gamma+d\rightarrow K^{+}+\Lambda+n$ that includes both impulse and rescattering contributions. Most of the well-established resonances of spins $\frac{1}{2}$ and $\frac{3}{2}$ below 1.9 GeV are incorporated in the model. Initial estimates for the relevant coupling strengths are extracted from empirical information and SU(3) symmetry relations. For certain resonances, these initial estimates are modified to bring the cross sections calculated for certain elementary processes related to the rescattering terms in rough qualitative agreement with the empirical cross sections for these processes. For the N^{*} and Δ resonances included in the model, off-shell width extrapolations are obtained by treating the energy and momentum dependence of each decay channel separately. Since the main intent of the study is to ascertain the importance of the rescattering terms in the reaction amplitudes, no attempt has been made to include final state correlations. To represent the initial state, a nonrelativistic deuteron wave function is employed. Results are presented for the differential cross section in the deuteron rest frame at fixed kaon energy and angle. The results indicate that rescattering contributions to the photoproduction of kaons from the deuteron may be significant over a wide kinematical range.

DOI: 10.1103/PhysRevC.69.034605 PACS number(s): 25.10.+s, 25.20.Lj, 13.60.−r

I. INTRODUCTION

Electromagnetic production of mesons from light nuclei has long been of interest in nuclear physics as a means of studying baryon-baryon interactions. A major advantage of such reactions over reactions involving strong interaction probes is that the electromagnetic part of the reaction can be treated perturbatively.

While there exists a fairly extensive literature concerning pion photoproduction and electroproduction from light nuclei, such as the deuteron [1,2] and ^{3}He [3], it has only been comparatively recently that kaon electromagnetic production from light nuclei has received much attention. Detailed studies of kaon electromagnetic production are of interest for several reasons. They provide information concerning the hyperon-nucleon interaction in a different kinematical region from that accessible in hypernuclear studies, and thus expand our knowledge of that important interaction. Because kaons involve the strangeness degree of freedom, reactions involving kaons also provide information concerning the quark-gluon interaction that cannot be obtained from pion reactions alone. Finally, kaon production provides a new arena for testing reaction models for electromagnetic meson production.

Prior to the late 1980s, virtually all the theoretical studies of kaon electromagnetic production were carried out for proton targets. Among the earliest of these are the work of Thom [4] and Renard and Renard [5]. Subsequently, a number of groups performed exhaustive semiphenomenological analyses of the existing photoproduction and electroproduction data using an effective Lagrangian approach [6–12]. The major difficulty with this approach is that the data do not adequately constrain the resonances included in the fits. Different analyses achieve comparable fits using quite different sets of resonances, so that the reliability of the resulting coupling strength determinations is not clear. Recently, the Ghent group has studied a number of issues related to electromagnetic production of strangeness from the proton [13].

Kaon photoproduction from the deuteron was first studied in detail by Renard and Renard [14] within a one-body reaction model (impulse approximation) supplemented by final state interactions. Due to a paucity of data, there was little further work on photoproduction from the deuteron until the construction of CEBAF made the acquisition of new high quality data possible. Most of the recent theoretical work employs a reaction model similar to that of Renard and Renard and focuses primarily on the role of final state interactions [15–17]. The model has recently been extended to a treatment of kaon photoproduction from ^{3}He [18] with the emphasis again on final state interactions.

While the role of final state interactions in kaon photoproduction is certainly a very significant question, the reaction mechanism itself also deserves attention. Within the one-body reaction model, a single nucleon absorbs the incident photon and emits the outgoing kaon. However, to conserve momentum in the reaction, momentum has to be transferred between the outgoing baryons. Because of the lack of high momentum components in the deuteron, the only effective mechanism for achieving this in the one-body model is through the final state interaction. When the outgoing baryons have small relative momentum, they can interact strongly, and final state interactions are effective in transferring momentum between the outgoing baryons. However, when the relative momentum is not small, the final state interaction falls off rapidly, and with it the calculated cross section.

The inclusion of two-body terms in the reaction mechanism, in which different nucleons absorb the photon and emit the kaon, could alter this result significantly. These two-body terms involve an explicit meson exchange between the participating baryons and thus provide an additional momentum transfer mechanism. Laget has shown, in the case of pion photoproduction from the deuteron, that such rescattering terms can make significant contributions to the cross section in certain kinematical regimes [2]. In the work described here, we examine the contributions of rescattering terms in kaon photoproduction.

A related question, which has not received much attention in the literature, is the dependence of the deuteron kaon photoproduction results on the input coupling strengths. As discussed above, it is possible to achieve comparable fits to the data for photoproduction from the proton using quite different sets of intermediate resonances. In the impulse approximation one might expect these different resonance sets to yield similar results for the deuteron reaction since in that approximation, the reaction mechanisms for the deuteron reaction and the proton reaction are essentially the same. This is not the case, however, when two-body contributions are included, which suggests that a careful examination of the deuteron data away from threshold may allow one to distinguish between different fits to the proton data.

In Sec. II of this work, a model for the reaction

$$\gamma + d \rightarrow K^+ + \Lambda + n \tag{1}$$

is presented which contains both one-body (impulse) and two-body (rescattering) terms. Section II enumerates the set of intermediate resonances incorporated in the model and contains a detailed discussion of the resonance propagators and interaction vertices that are employed.

Section III outlines the procedure employed for the determination of the coupling strengths and phases associated with the various interaction vertices. In most previous work, these coupling strengths and phases have just been taken from one of the fits to the proton data. Two considerations make this procedure unsatisfactory for the calculations described here. First, as mentioned above, different fits to the proton data involve quite different sets of resonances. While the various fits presumably give similar results for the impulse contributions to the deuteron reaction, they might yield rather different results for the rescattering contributions to the deuteron reaction. Since there does not appear to be any compelling reason to regard one fit as superior to the others, one is faced with the problem of deciding which fit to use.

A second more serious problem is that the rescattering terms involve couplings that are not determined at all in the proton fits. For example, the rescattering terms have contributions from intermediate Δ resonances that do not occur in the impulse terms. Evaluation of the rescattering terms also requires knowledge of π-baryon and η-baryon coupling strengths that are not determined in the proton fits. We bypass these difficulties by relying on other data sources and on symmetry relations to estimate the coupling strengths and phases required in the model. The quality of the resulting coupling strengths is tested by using them to evaluate the cross sections for certain related elementary processes, in particular, kaon-nucleon elastic scattering, the reaction $\pi^- p \rightarrow K^0 \Lambda$, and photoproduction of the Λ from the proton, and then comparing with empirical curves generated using the SAID facility [19]. This procedure reveals the need for some adjustments, as discussed in Sec. III.

In addition to coupling strengths, values are required for the widths of the nonstrange resonances included in the model. Wherever possible, empirical information has been employed to fix the widths on the mass shell. However, the widths are usually needed quite far off the mass shell, making it necessary to develop a model for the energy and momentum dependence of the widths. This model is described in some detail in Sec. IV.

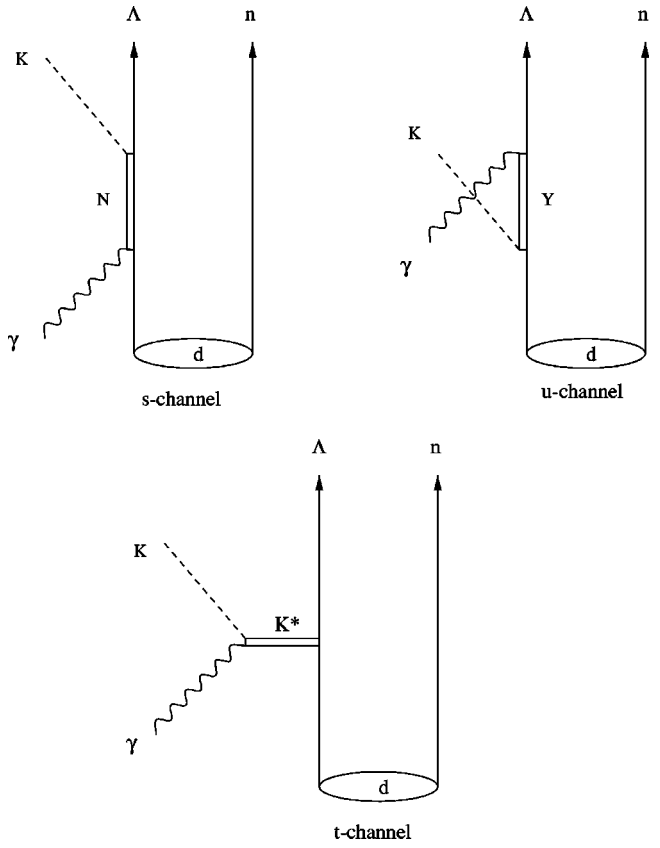

FIG. 1. Impulse contributions to the reaction amplitude.

The matrix element for the reaction (1) must be evaluated between an initial deuteron state and a three-body final state. In principle, a relativistic deuteron wave function should be employed for the initial state and all possible interactions included in the final state. In practice, a more modest calculation has been performed using a nonrelativistic deuteron wave function and neglecting final state interactions. The major effect of relativity on the deuteron is to introduce small p-wave components in the wave function. The effect of these small components on kaon photoproduction has been studied within the impulse approximation in a previous work and found to be relatively unimportant [15]. Details concerning the evaluation of the matrix elements are contained in Sec. V. Numerical results for the photoproduction cross section are presented and discussed in Sec. VI.

II. THE REACTION MODEL

The contributions to the reaction model included in the present work are depicted diagrammatically in Figs. 1 and 2. In addition to the diagrams shown, there is a second set of diagrams with the photon absorbed on the right which must be included to correctly account for the deuteron isospin. These additional diagrams need not be evaluated explicitly, however, since their amplitudes are identical to those depicted in the figures. They can be incorporated by just dou-

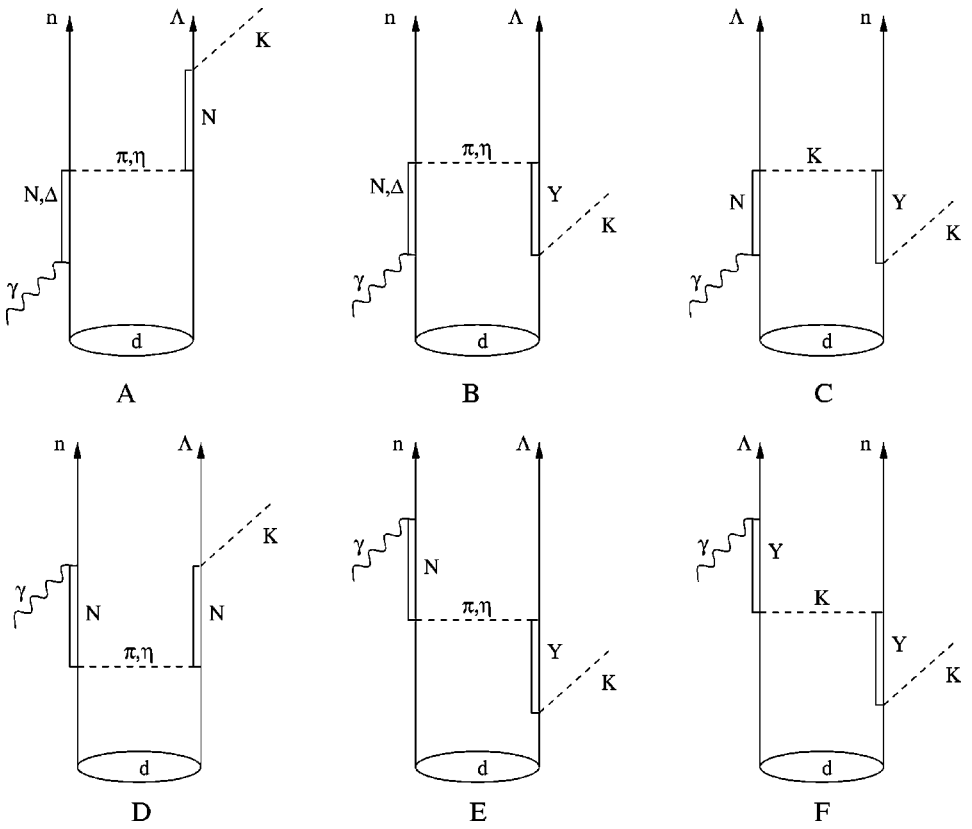

FIG. 2. Rescattering contributions to the reaction amplitude.

bling the calculated matrix elements. Together with a factor $1/\sqrt{2}$ from the deuteron isospin, this yields an overall factor of 2 in the cross section as compared with a calculation that does not account for the deuteron isospin.

Figure 1 depicts the usual *s*-channel, *u*-channel, and *t*-channel contributions to the amplitude in the impulse approximation. Note that the Born terms, in which the intermediate lines in the *s*- and *u*-channel contributions are ground state baryons, have been included in these diagrams.

Figure 2 depicts the rescattering contributions included in the present analysis. These diagrams represent all possible rescattering contributions with one intermediate resonance excitation on each baryon line. The exchanged meson can be either neutral or charged depending upon whether the nucleon on the left is a proton or a neutron. Since the deuteron has isospin zero, the neutral exchange contributions have to be subtracted from, rather than added to, the charge exchange contributions. It should be noted that the zero isospin of the deuteron precludes the excitation of Δ resonances in either of diagrams (d) or (e).

We have made no attempt to include vector meson exchange in the rescattering amplitudes. The incorporation of vector meson exchange would not only complicate those amplitudes considerably, but it would require a host of additional coupling strengths that are difficult to determine. Even more significantly, vector meson exchanges involve the relative phases between vector meson-baryon-resonance vertices and pseudoscalar-baryon-resonance vertices. SU(3) symmetry relations are of no help in determining these phases since they do not connect the couplings of mesons in different SU(3) multiplets. The same situation regarding coupling strengths and phases applies to σ exchange as well, so σ exchange terms in the rescattering amplitudes have not been included in the model. By contrast, the pseudoscalar exchange contributions involve only the phases of the photon interactions relative to the pseudoscalar meson interactions, which can generally be fixed with the aid of empirical photoproduction amplitudes and SU(3).

We include a much larger set of resonances in the present work than has been incorporated in most previous work. This is made necessary by the fact that resonances that do not have much effect in the impulse approximation can, in principle, have a large effect in the rescattering terms. In the impulse terms, a resonance must couple strongly to both the photon and the kaon to have a significant impact on the amplitude, but in the rescattering terms *different* resonances are associated with the photon absorption and kaon emission vertices. Thus, resonances need to be included which interact strongly with the kaon but may not interact strongly with the photon. This discussion should also make clear that the coupling strengths at the photon vertices and at the pseudoscalar meson vertices need to be known *separately*. The coupling strengths determined in the proton fits, which are actually products of the coupling strengths at the photon and kaon vertices, are of little utility in evaluating the rescattering amplitudes.

Ideally, our analyses should incorporate all the well-established resonances (those of three or four star status in the particle data tables) below some maximum energy. In practice, one can include only those resonances for which the required interaction strengths and phases can be estimated with some degree of reliability. This restriction effectively rules out most of the resonances above a rest energy of 1.9 GeV or so. Above this energy, there is little width or

TABLE I. Resonances included in the model.

Resonance	I	J^P	SU(6)	SU(3)
$N(1440)$	$\frac{1}{2}$	$\frac{1}{2}^+$	$56,0^+$	$^2 8$
$N(1520)$	$\frac{1}{2}$	$\frac{3}{2}^-$	$70,1^-$	$^2 8$
$N(1535)$	$\frac{1}{2}$	$\frac{1}{2}^-$	$70,1^-$	$^2 8$
$N(1650)$	$\frac{1}{2}$	$\frac{1}{2}^-$	$70,1^-$	$^4 8$
$N(1700)$	$\frac{1}{2}$	$\frac{3}{2}^-$	$70,1^-$	$^4 8$
$N(1710)$	$\frac{1}{2}$	$\frac{1}{2}^+$	$70,0^+$	$^2 8$
$N(1720)$	$\frac{1}{2}$	$\frac{3}{2}^+$	$56,2^+$	$^2 8$
$\Delta(1232)$	$\frac{3}{2}$	$\frac{3}{2}^+$	$56,0^+$	$^4 10$
$\Delta(1600)$	$\frac{3}{2}$	$\frac{3}{2}^+$	$56,0^+$	$^4 10$
$\Delta(1620)$	$\frac{3}{2}$	$\frac{1}{2}^-$	$70,1^-$	$^2 10$
$\Delta(1700)$	$\frac{3}{2}$	$\frac{3}{2}^-$	$70,1^-$	$^2 10$
$\Lambda(1405)$	0	$\frac{1}{2}^-$	$70,1^-$	$^2 1$
$\Lambda(1520)$	0	$\frac{3}{2}^-$	$70,1^-$	$^2 1$
$\Lambda(1600)$	0	$\frac{1}{2}^+$	$56,0^+$	$^2 8$
$\Lambda(1670)$	0	$\frac{1}{2}^-$	$70,1^-$	$^4 8$
$\Lambda(1690)$	0	$\frac{3}{2}^-$	$70,1^-$	$^2 8$
$\Lambda(1810)$	0	$\frac{1}{2}^+$	$70,0^+$	$^2 8$
$\Lambda(1890)$	0	$\frac{3}{2}^+$	$56,2^+$	$^2 8$
$\Sigma(1385)$	1	$\frac{3}{2}^+$	$56,0^+$	$^4 10$
$\Sigma(1660)$	1	$\frac{1}{2}^+$	$56,0^+$	$^2 8$
$\Sigma(1670)$	1	$\frac{3}{2}^-$	$70,1^-$	$^2 8$
$\Sigma(1750)$	1	$\frac{1}{2}^-$	$70,1^-$	$^2 10$

photoamplitude data available, and uncertain multiplet assignments limit the applicability of SU(3) symmetry relations. We have further restricted the resonances considered to those with spins of $\frac{1}{2}$ or $\frac{3}{2}$, mainly to avoid complications associated with the vertex functions and propagators of higher spin states. There are only a few well-established resonances with spins greater than $\frac{3}{2}$ below 1.9 GeV; their exclusion should not qualitatively affect the results obtained.

A list of all the resonances incorporated in the present work is given in Table I. The spin-parity assignments in the third column have been taken from the particle data tables [20], while the symmetry assignments in columns 4 and 5 are consistent with those used in $\mathrm{SU}(6)\times\mathrm{O}(3)$ analyses of spectra and decay rates [21,22].

As discussed above, the impulse amplitude consists of the s-channel, u-channel, and t-channel exchanges represented by the diagrams depicted in Fig. 1. These amplitudes have the general forms

$$\hat{T}_s = \sum_R \mathcal{V}_K^\dagger(p_K) D_R(p_R) \mathcal{V}_\gamma(p_\gamma), \tag{2}$$

$$\hat{T}_u = \sum_R \mathcal{V}_\gamma^\dagger(p_\gamma) D_R(p'_R) \mathcal{V}_K(p_K), \tag{3}$$

and

$$\hat{T}_t = \sum_{K^\star} \mathcal{V}_{\gamma K}^\dagger(p_\gamma, p_{K^\star}) D_{K^\star}(p_{K^\star}) \mathcal{V}_{p\Lambda}(p_{K^\star}), \tag{4}$$

where $p_R = p_\Lambda + p_K$ and $p'_R = p_\Lambda - p_\gamma$ are the resonance 4-momenta in the s-channel and u-channel terms, respectively, and $p_{K^\star}$ is the 4-momentum carried by the kaon resonance in the t-channel term. The $\mathcal{V}$'s here denote vertex functions, while the D's denote intermediate resonance propagators. In the s-channel term, the intermediate resonance sum includes the nucleon and all $N^\star$ resonances incorporated in the model; in the u-channel term, the sum includes the ground state Λ and Σ and all $Y^\star$ resonances incorporated in the model; and in the t-channel term, the sum includes the $K^\star(892)$ and the $K1(1270)$ resonances, which have been incorporated in previous analyses.

The vertex functions and intermediate propagators appearing in the s- and u-channel impulse amplitudes are of the same form as those employed in the rescattering terms and are discussed below. The t-channel vertex functions are given by

$$\mathcal{V}_{\gamma K}^\mu = \frac{g_{\gamma K K^\star}}{m_{sc}} \epsilon^{\mu\nu\rho\lambda} \epsilon_\nu p_{\gamma\rho} p_{K^\star\lambda} \tag{5}$$

and

$$\mathcal{V}_{p\Lambda}^\mu = \left(g_{p\Lambda K^\star}^V + \frac{g_{p\Lambda K^\star}^T}{m_p + m_\Lambda} \gamma \cdot p_{K^\star} \right) \gamma^\mu \tag{6}$$

for the $K^\star(892)$ resonance and

$$\mathcal{V}_{\gamma K}^\mu = \frac{g_{\gamma K K1}}{m_{sc}} (\epsilon \cdot p_{K1} p_\gamma^\mu - p_\gamma \cdot p_{K1} \epsilon^\mu) \tag{7}$$

and

$$\mathcal{V}_{p\Lambda}^\mu = \left(g_{p\Lambda K1}^V + \frac{g_{p\Lambda K1}^T}{m_p + m_\Lambda} \gamma \cdot p_{K1} \right) \gamma^\mu \gamma_5 \tag{8}$$

for the $K1(1270)$ resonance, where m_{sc} is a scaling mass that we set equal to 1000 MeV. The two kaon resonances have propagators of the same form,

$$D_{K^\star} = \frac{-g_{\mu\nu} + \dfrac{p_{K^\star\mu} p_{K^\star\nu}}{m_{K^\star}^2}}{p_{K^\star}^2 - m_{K^\star}^2 + i m_{K^\star} \Gamma_{K^\star}}, \tag{9}$$

where now the label $K^\star$ refers to either of the two resonances.

The rescattering terms are given by the general expressions

$$\hat{T}_A = \hat{T}_{\gamma d} G_{\pi,\eta}(q) \hat{T}_{Kd},$$

$$\hat{T}_B = \hat{T}_{\gamma d} G_{\pi,\eta}(q) \hat{T}_{Kc},$$

$$\hat{T}_C = \hat{T}_{\gamma d} G_K(q) \hat{T}_{Kc},$$

$$\hat{T}_D = \hat{T}_{\gamma c} G_{\pi,\eta}(q) \hat{T}_{Kd},$$

$$\hat{T}_E = \hat{T}_{\gamma c} G_{\pi,\eta}(q) \hat{T}_{Kc},$$

$$\hat{T}_F = \hat{T}_{\gamma c} G_K(q) \hat{T}_{Kc}, \tag{10}$$

each of which contains a factor involving the absorbed photon (hereafter, termed the photon absorption amplitude), a factor involving the emitted kaon (hereafter, termed the kaon emission amplitude), and a propagator for the exchange of either a nonstrange meson (labeled π, η) or a kaon. The direct and crossed photon absorption amplitudes (identified with subscripts d and c) have the same structure as the s- and u-channel impulse amplitudes, respectively, except for additional meson vertex form factors to account for the off-shell nature of the exchanged mesons. The meson propagators and kaon emission amplitudes have the forms

$$G_M = \frac{1}{q^2 - m_M^2}, \tag{11}$$

where m_M and q are the meson mass and 4-momentum, and

$$\hat{T}_{Kd} = \sum_R \mathcal{V}_K^\dagger(p_K) D_R(p_R) \mathcal{V}_M(p_M),$$

$$\hat{T}_{Kc} = \sum_R \mathcal{V}_M^\dagger(p_M) D_R(p_R') \mathcal{V}_K(p_K), \tag{12}$$

where the $\mathcal{V}_M$'s are the interaction vertices associated with the exchanged mesons and include off-shell form factors.

The vertex functions and resonance propagators appearing in these expressions depend upon the spin and parity of the excited resonance. For spin $\frac{1}{2}$ resonances, we employ the standard spin $\frac{1}{2}$ photon vertex function and use the pseudoscalar version of the meson vertex function. This gives for the positive parity resonances (with form factors not shown)

$$\mathcal{V}_{K(1/2^+)}(p_K) = g \gamma_5 \tag{13}$$

and

$$\mathcal{V}_{\gamma(1/2^+)}(p_\gamma) = g_\gamma \epsilon_\mu i \sigma^{\mu\nu} (p_\gamma)_\nu \tag{14}$$

with

$$g_\gamma = \frac{e\kappa}{2m_B}, \tag{15}$$

where m_B is the mass of the ground state baryon participating in the interaction, and the parameter κ is defined by its relation to the transition magnetic moment,

$$\mu_T = \frac{e\kappa}{m_B + m_R}. \tag{16}$$

If the intermediate baryon is a proton, the photon vertex contains an additional charge term, $e\gamma^\mu (p_\gamma)_\mu$. The negative parity spin $\frac{1}{2}$ vertex functions are given by similar expressions but with the γ_5 factor occurring in the photon vertex function rather than in the kaon vertex function.

For the spin $\frac{1}{2}$ propagator, we employ a relativistic Breit-Wigner form

$$D^{1/2} = \frac{\gamma \cdot p_R + m_R}{p_R^2 - m_R^2 + i m_R \Gamma_R}, \tag{17}$$

where Γ_R is the resonance width. This form has been used in most of the previous photoproduction studies. However, Benmerrouche *et al.* have noted that Eq. (17) leads to inconsistent amplitudes in different partial waves and hence, violates unitarity [23]. A better procedure would be to generate the imaginary part of the t-matrix explicitly through a K-matrix approach. This requires the solution of coupled channel equations, however, and would be technically very difficult in the present case which involves a large number of resonances coupled to many different channels.

For the spin $\frac{3}{2}$ propagator, we make use of the Rarita-Schwinger form consisting of the spin $\frac{1}{2}$ propagator multiplied on the right by the operator

$$P_{\mu\nu} = g_{\mu\nu} - \frac{1}{3}\gamma_\mu \gamma_\nu + \frac{1}{3}\frac{(p_R)_\mu \gamma_\nu - (p_R)_\nu \gamma_\mu}{m_R} - \frac{2}{3}\frac{(p_R)_\mu (p_R)_\nu}{m_R^2}. \tag{18}$$

This differs from the propagator used in Ref. [6]. To ensure gauge invariance, the authors of that reference replace the masses in Eq. (18) and in the numerator of the Feynman propagator by $\sqrt{s}$. However, the resulting form does not satisfy the differential equation that defines the propagator, as shown in Ref. [23]. Moreover, as noted in Ref. [12], it introduces unphysical singularities in the u-channel where $\sqrt{s}$ can vanish. Recent work [12,23,24] has shown that the correct gauge invariant treatment of spin $\frac{3}{2}$ particles requires the incorporation of additional off-shell structure in the spin $\frac{3}{2}$ interaction Lagrangians. We have made no attempt to include this off-shell structure here, as we have no means of estimating the associated parameters. We note, however, that the off-shell structure could have a significant impact in rescattering processes where the intermediate resonances can be quite far off-shell, especially in the u channel.

With off-shell terms omitted, the spin $\frac{3}{2}$ interaction vertices reduce to those used in Ref. [12] with the θ functions replaced by the metric tensor. In particular, for the positive parity resonances, we have (with form factors suppressed)

$$\mathcal{V}^\mu_{K(3/2^+)}(p_K) = -\frac{g}{m_\pi} p_K^\mu, \tag{19}$$

where the factor m_π has been included to make g dimensionless, and

$$\mathcal{V}^\mu_{\gamma(3/2^+)}(p_\gamma) = \left[\frac{g_1}{2m_B}(\epsilon^\mu \gamma \cdot p_\gamma - p_\gamma^\mu \gamma \cdot \epsilon) + \frac{g_2}{4m_B^2}(\epsilon \cdot p_B p_\gamma^\mu - p_\gamma \cdot p_B \epsilon^\mu) \right] \gamma_5, \tag{20}$$

where p_B is the 4-momentum of the ground state baryon participating in the interaction. The negative parity vertex functions are given by similar expressions but with the γ_5 factor occurring in the kaon vertex function rather than in the

photon vertex function. The spin $\frac{3}{2}$ propagator is given by the expression

$$D^{3/2}_{\mu\nu} = \frac{\gamma \cdot p_R + m_R}{p_R^2 - m_R^2 + i m_R \Gamma_R} P_{\mu\nu}, \tag{21}$$

with $P_{\mu\nu}$ defined by Eq. (18).

III. COUPLING STRENGTHS AND PHASES

To evaluate the amplitudes discussed above, the various coupling strengths must be assigned values. For the *t*-channel impulse term, we need the products of the photon coupling strengths with the vector and tensor baryon coupling strengths. For these products we employ the values

$$g_{p\Lambda K^\star} g^V_{\gamma K K^\star} = -2.01,$$

$$g_{p\Lambda K^\star} g^T_{\gamma K K^\star} = 1.00,$$

$$g_{p\Lambda K1} g^V_{\gamma K K1} = 0.25,$$

$$g_{p\Lambda K1} g^V_{\gamma K K1} = 2.13, \tag{22}$$

which are just those given in Ref. [11].

For the rescattering terms, we need the coupling strengths at the photon vertices and the meson vertices separately. Thus, we cannot just use the results from one of the proton fits, since these fits give only the product of the two coupling strengths, not the coupling strengths individually. We could, of course, adopt one of the proton fits for the impulse terms, where only the coupling strength products are required, and then employ a different prescription for the rescattering terms, but for the sake of consistency, we have rejected this approach. Instead we determine the two sets of couplings independently. For each type of vertex, we first derive a preliminary set of coupling strengths and use these to calculate the cross sections for a number of elementary processes that are related to the rescattering contributions depicted in Fig. 2. We then make adjustments in individual coupling strengths so as to make the calculated cross sections resemble the empirical ones as closely as possible within the model adopted.

In connection with the meson vertices, we examine the amplitudes for K^+p and K^+n elastic scattering and the amplitude for the reaction

$$\pi^- + p \rightarrow K^0 + \Lambda. \tag{23}$$

Contributions to these processes are shown in Fig. 3. Note that we have only considered contributions that are specifically related to the rescattering diagrams depicted in Fig. 2. There are additional contributions to these processes that we have not considered since they are not related to the rescattering diagrams in Fig. 2, and consequently, we should not expect to reproduce the empirical cross sections for these processes too closely.

In connection with the photon vertices, we examine the amplitude for strangeness photoproduction from the proton,

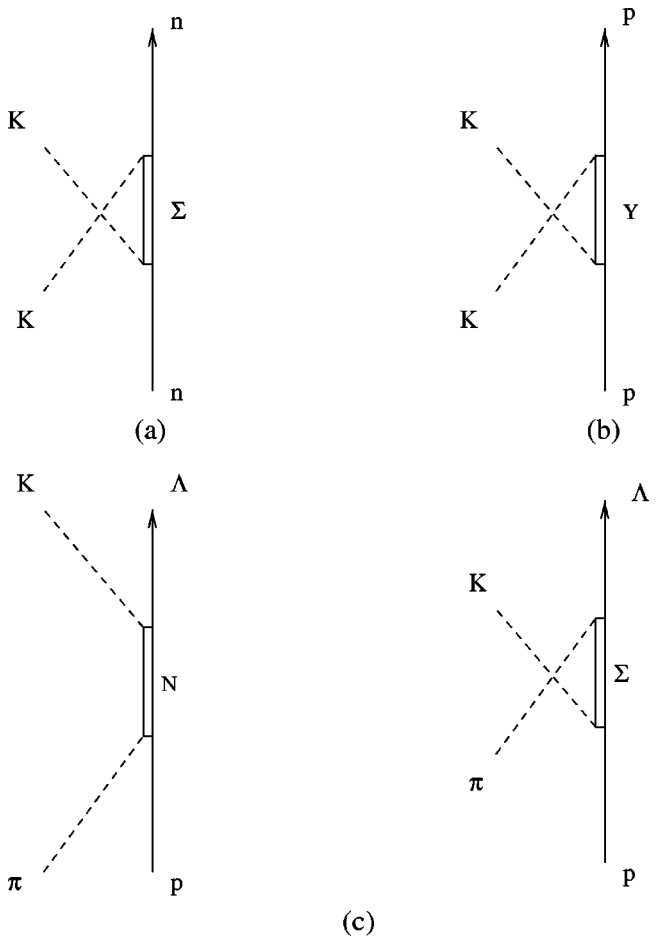

FIG. 3. Contributions to the amplitudes for (a) K^+n elastic scattering, (b) K^+p elastic scattering, and (c) the reaction $\pi^-p \rightarrow K^0\Lambda$.

$$\gamma + p \rightarrow K^+ + \Lambda. \tag{24}$$

Contributions to this process are depicted in Fig. 4. In contrast with the cross sections for the mesonic processes discussed above, we should be able to reproduce the cross section for this process fairly well.

We first consider the meson couplings, which depend upon both the quantum numbers of the particular resonance considered and on whether that resonance is excited or deexcited at the meson-baryon-resonance vertex. Since we only treat the photoproduction of the Λ, we need not consider any couplings that involve a Σ in the final state. Thus, with the restriction to pseudoscalar meson exchange, there are only three meson coupling strengths required for each resonance, involving a π, an η, or a K or $\overline{K}$.

The isospin symmetry of the strong interaction allows us to express these couplings as products of an SU(2) isospin coupling coefficient and an SU(3) isoscalar factor. In the baryon first convention,

$$g(BM \rightarrow R) = (I_B \lambda_B I_M \lambda_M | I_R \lambda_R) f_{BM:R} \tag{25}$$

at vertices where a resonance is excited and

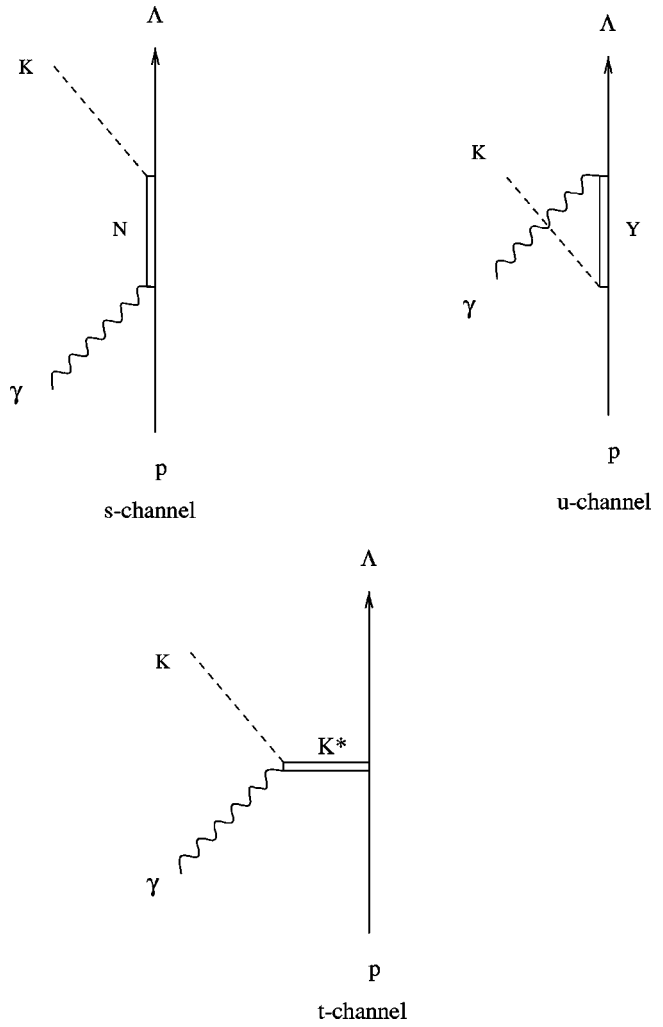

FIG. 4. Contributions to the amplitude for the reaction $\gamma p \rightarrow K^+\Lambda$.

$$g(RM \rightarrow B) = (I_R \lambda_R I_M \lambda_M | I_B \lambda_B) f_{RM:B} \tag{26}$$

at vertices where a resonance is deexcited. The I's and λ's here are isospins and isospin projections, and the various hadrons involved in the interaction are identified by the labels B (ground state baryon), M (pseudoscalar meson), and R (resonance).

The meson couplings can be further constrained if it is assumed that the overall coupling strength associated with a given resonance multiplet does not depend on whether the resonances are excited or deexcited in the interaction. Then the isoscalar factors associated with resonance excitation and deexcitation are connected by SU(3) symmetry. In particular, using the tables compiled in Ref. [28], we obtain the relations

$$f_{N^\star \pi:N} = f_{N\pi:N^\star},$$

$$f_{\Sigma^\star \pi:\Lambda} = -\sqrt{3} f_{\Lambda\pi:\Sigma^\star},$$

$$f_{N^\star \eta:N} = f_{N\eta:N^\star},$$

$$f_{\Lambda^\star \eta:\Lambda} = f_{\Lambda\eta:\Lambda^\star},$$

$$f_{\Lambda^\star K:N} = -\sqrt{\frac{1}{2}} f_{N\bar{K}:\Lambda^\star},$$

$$f_{\Sigma^\star K:N} = \sqrt{\frac{3}{2}} f_{N\bar{K}:\Sigma^\star} \tag{27}$$

for SU(3) octets,

$$f_{\Lambda^\star \eta:\Lambda} = -2\sqrt{2} f_{\Lambda\eta:\Lambda^\star},$$

$$f_{\Lambda^\star K:N} = 2 f_{N\bar{K}:\Lambda^\star} \tag{28}$$

for singlets, and

$$f_{\Delta\pi:N} = \frac{2}{5}\sqrt{10} f_{N\pi:\Delta},$$

$$f_{\Sigma^\star \pi:\Lambda} = \frac{2}{5}\sqrt{15} f_{\Lambda\pi:\Sigma^\star},$$

$$f_{\Sigma^\star K:N} = -\frac{1}{5}\sqrt{30} f_{N\bar{K}:\Sigma^\star} \tag{29}$$

for decuplets. These relations can be used to fix the resonance deexcitation isoscalar factors in terms of the resonance excitation factors.

Wherever possible we use experimental information to obtain estimates for the remaining isoscalar factors. Where experimental information is lacking, we resort to SU(3) symmetry relations. SU(3) symmetry relations are also employed to fix the relative phases of different couplings within the same SU(3) multiplet. For SU(3) octets, these relations can be expressed in the form [28]

$$f_{N\pi:N^\star} = f_0,$$

$$f_{N\eta:N^\star} = \left(1 - \frac{4}{3}\alpha\right) f_0,$$

$$f_{\Lambda K:N^\star} = -\left(1 - \frac{2}{3}\alpha\right) f_0,$$

$$f_{N\bar{K}:\Lambda^\star} = \sqrt{2}\left(1 - \frac{2}{3}\alpha\right) f_0,$$

$$f_{N\bar{K}:\Sigma^\star} = \frac{\sqrt{6}}{3}(1 - 2\alpha) f_0,$$

$$f_{\Sigma\pi:\Lambda^\star} = -\frac{2}{3}\sqrt{3}\alpha f_0,$$

$$f_{\Lambda\pi:\Sigma^\star} = -f_{\Lambda\eta:\Lambda^\star} = \frac{2}{3}\alpha f_0, \tag{30}$$

involving the two parameters f_0 and α. The corresponding relations for singlets,

$$f_{N\bar{K}:\Lambda^\star} = \frac{\sqrt{6}}{3} f_{\Sigma\pi:\Lambda^\star},$$

$$f_{\Lambda\eta:\Lambda^\star} = -\frac{\sqrt{3}}{3} f_{\Sigma\pi:\Lambda^\star},$$

$$f_{\Lambda\eta:\Lambda^\star} = -\frac{\sqrt{2}}{2} f_{N\bar{K}:\Lambda^\star}, \tag{31}$$

and decuplets,

$$f_{N\bar{K}:\Sigma^\star} = -f_{\Sigma\pi:\Sigma^\star}$$

$$f_{\Lambda\pi:\Sigma^\star} = -\frac{\sqrt{6}}{2} f_{\Sigma\pi:\Sigma^\star}, \tag{32}$$

each involve just a single parameter.

For the ground state baryon octet, we use the values given in Ref. [29] to fix the pion couplings and then use Eqs. (30) to fix the kaon and η meson couplings. This yields a preliminary set of values given by

$$f_{N\pi:N} = 23.3,$$

$$f_{\Lambda\pi:\Sigma} = 12.3,$$

$$f_{N\eta:N} = 3.88,$$

$$f_{\Lambda\eta:\Lambda} = -12.3,$$

$$f_{\Lambda K:N} = -13.6,$$

$$f_{N\bar{K}:\Lambda} = 19.2,$$

$$f_{N\bar{K}:\Sigma} = -4.76. \tag{33}$$

For resonances the isoscalar factors are related to the widths for decays into particular pseudoscalar meson ground state baryon channels. For the pseudoscalar meson interactions defined previously, these widths are given in the resonance rest frame by

$$\Gamma\left(\frac{1^P}{2} \to \frac{1^+}{2} + 0^-\right) = \frac{f^2}{4\pi}\frac{p}{\sqrt{s}}[E_B - \eta_P m_B] \tag{34}$$

for spin $\frac{1}{2}$ resonances and by

$$\Gamma\left(\frac{3^P}{2} \to \frac{1^+}{2} + 0^-\right) = \frac{1}{12\pi}\frac{f^2}{m_\pi^2}\frac{p^3}{\sqrt{s}}[E_B + \eta_P m_B] \tag{35}$$

for spin $\frac{3}{2}$ resonances, where p is the channel momentum and E_B is the ground state baryon energy. Equations (34) and (35) yield estimates for the magnitudes of the corresponding isoscalar factors for decay channels with reasonably well determined branching ratios. These include the $N\pi$ decay channels of the nonstrange resonances and most of the $N\bar{K}$ or ΛK decay channels of the strange resonances that lie above the corresponding thresholds. By contrast, most of the $\Lambda\pi$ and η baryon branching ratios are not known.

To obtain preliminary estimates for those isoscalar factors not fixed by the width data and to fix the relative phases of the isoscalar factors, we employ the SU(3) symmetry relations given previously. For the octet resonances, two input couplings are required for each octet to fix the remaining couplings within that octet. The selection of these input couplings is motivated by the expectation that decay channels with similar total masses are more likely to satisfy SU(3) constraints than are decay channels with widely divergent masses. Whether this expectation is actually realized in practice is not clear, but it does give a definite prescription for fixing isoscalar factors. Thus, for the two low lying $\frac{1^+}{2}$ octets, we use empirical values for the $N\bar{K}\Lambda^\star$ and $N\bar{K}\Sigma^\star$ couplings to provide estimates for the $\Lambda K N^\star$, $\Lambda\pi\Sigma^\star$, and η couplings where needed. For octets where the Σ resonance is missing, we use the $\Sigma\pi\Lambda^\star$ coupling as input instead of the $N\bar{K}\Sigma^\star$ coupling, and for the two octets which contain just an $N^\star$ resonance, we use the $N\pi N^\star$ and $N\eta N^\star$ couplings as input.

For singlet and decuplet resonances, only one input coupling is required. We use the $\Sigma\pi\Sigma^\star$ coupling as input to provide estimates of the $N\bar{K}\Sigma(1385)$ and $\Lambda\pi\Sigma(1750)$ couplings, use the $\Sigma\pi\Lambda(1405)$ coupling to provide estimates of the $N\bar{K}\Lambda(1405)$ and $\Lambda\eta\Lambda(1405)$ couplings, and use the $N\bar{K}\Lambda(1520)$ coupling to provide an estimate of the $\Lambda\eta\Lambda(1520)$ coupling.

Using these coupling estimates, we then calculated the cross sections for the three mesonic processes represented in Fig. 3. The amplitudes for these processes have the same form as the kaon emission amplitudes discussed previously but without form factors. In the center of mass (c.m.), the cross sections are given by the general expression

$$\frac{d\sigma}{d\Omega} = \frac{1}{(2\pi)^2}\frac{m_I m_F q_F}{4 q_I s}\frac{1}{2}\sum_{spins}|\langle F|\hat{T}|I\rangle|^2, \tag{36}$$

where m_I and m_F are the incident nucleon and outgoing baryon masses, q_I and q_F are the 3-momenta of the incident and outgoing mesons, and s is the square of the total c.m. energy.

A comparison of the calculated cross sections with empirical cross sections [19] revealed a need for modifications in the preliminary set of couplings used. We considered the K^+n elastic scattering results first, since the calculated cross section for this process depends only on the kaon couplings to the Σ and $\Sigma^\star$ resonances. To get the right magnitude for the K^+n elastic cross section, we had to increase the magnitude of the $\Sigma(1660)$ coupling by a factor of 1.8 and to slightly modify the $\Sigma(1385)$ and $\Sigma(1670)$ couplings.

Next, we considered K^+p elastic scattering. The calculated cross section for this process depends on the kaon couplings of both Σ and Λ resonances. The $\Sigma^\star$ couplings have already been modified through consideration of K^+n elastic scattering, so we employed K^+p elastic scattering to test the Λ and $\Lambda^\star$ couplings. We find that the original choices for these couplings make the K^+p elastic cross section much too large.

To get the magnitude of this cross section correctly, we had to reduce the $N\bar{K}:\Lambda$ coupling by a factor of 4 and to eliminate the kaon coupling to the $\Lambda(1520)$ entirely. We also had to reduce the kaon coupling to the $\Lambda(1690)$ by a factor of 2 and to increase the kaon coupling to the $\Lambda(1600)$ by about 15%. It should be noted that the reduction of the $N\bar{K}:\Lambda$ coupling reduces the $\Lambda K:N$ coupling as well because of the relations given by Eq. (27).

Finally, we considered reaction (23), which we used to test the π couplings to the Σ resonances and the $K\Lambda$ couplings to the nucleon resonances. Like the K^+p elastic cross section, the calculated cross section for this process is much too large with the original coupling choices. To get the right order of magnitude for this cross section, it was necessary to reduce the π couplings to the Σ and the $\Sigma(1660)$ by factors of 2 and to suppress the π couplings to the $\Sigma(1385)$ and $\Sigma(1670)$ entirely. We also had to reduce the $K\Lambda$ coupling to the $N(1520)$ by a factor of 4.

The final set of isoscalar factors for the ground state baryons and all resonances are listed in Table II. The phases have been fixed by requiring that $f_{N\pi:N^\star}$, $f_{N\pi:\Delta}$ and the singlet $f_{\Sigma\pi:\Lambda^\star}$ all be positive.

Panels (a)–(c) of Fig. 5 display the resulting angular distributions for the three processes considered. In each panel the solid curve is the calculated cross section and the double solid curve the empirical cross section [19]. In the case of kaon-nucleon elastic scattering, the model gives the magnitudes of the empirical curves correctly, but not the shapes, while for reaction (23), the shape is correct but the calculated cross section too large. These discrepancies are most likely due to contributions to the elementary amplitudes that have not been included in the calculations. As discussed above, we have included only those contributions that are related to the rescattering diagrams in Fig. 2 and thus should not expect to achieve good fits to the empirical data for these three processes, no matter what coupling strengths are employed.

We turn now to the couplings at the photon vertices. Here the available data are much less extensive and less reliable than for the meson vertices. For the ground state baryons, the empirical magnetic moments given in Ref. [20] can be used to extract the κ values

$$\kappa_p = 2.793,$$

$$\kappa_n = -1.916,$$

$$\kappa_\Lambda = -0.729,$$

$$\kappa_{\Sigma\Lambda} = 1.91. \tag{37}$$

We found it necessary to modify the last of these to accommodate the empirical results for reaction (24), as discussed below.

For the nonstrange resonances, estimates of the photon couplings can be extracted from the empirical photodecay amplitudes, which are related to spin matrix elements of the photon vertex functions discussed in the preceding section. In particular, for the spin $\frac{1}{2}$ helicity matrix elements defined by

$$t^{M_R,M_B}_{1/2^P} = \bar{u}(M_B)\mathcal{V}_{\gamma(1/2^P)}u(M_R) \tag{38}$$

and for the spin $\frac{3}{2}$ matrix elements defined by

$$t^{M_R,M_B}_{3/2^P} = \bar{u}(M_B)\mathcal{V}^{\mu}_{\gamma(3/2^P)}u_\mu(M_R), \tag{39}$$

where P is the resonance parity and

$$u_\mu(M_R) = \sum_{M_1,M_2}\left(\frac{1}{2}M_1 1 M_2\middle|\frac{3}{2}M_R\right)u(M_1)\epsilon_\mu(M_2) \tag{40}$$

is the spin $\frac{3}{2}$ Rarita-Schwinger isobar, we have the relations

TABLE II. Meson isoscalar factors.

	$N^\star$ resonances		
	$f_{N\pi:N^\star}$	$f_{N\eta:N^\star}$	$f_{\Lambda K:N^\star}$
N	23.3	3.88	−3.4
$N(1440)$	11.355	−0.152	−4.028
$N(1520)$	2.714	−0.120	0.276
$N(1535)$	1.185	−2.025	0.420
$N(1650)$	1.452	0.525	−0.709
$N(1700)$	0.621	−0.628	0.004
$N(1710)$	1.808	0.832	−6.187
$N(1720)$	0.257	0.126	−0.512
	Δ resonances		
	$f_{N\pi:\Delta}$		
$\Delta(1232)$	2.201		
$\Delta(1600)$	0.507		
$\Delta(1620)$	0.849		
$\Delta(1700)$	1.317		
	Λ resonances		
	$f_{\Lambda\eta:\Lambda^\star}$	$f_{N\bar{K}:\Lambda^\star}$	
Λ	−12.3	4.8	
$\Lambda(1405)$	−0.912	1.289	
$\Lambda(1520)$	−3.017	0	
$\Lambda(1600)$	−4.181	6.95	
$\Lambda(1670)$	−1.152	0.447	
$\Lambda(1690)$	−1.358	0.779	
$\Lambda(1810)$	−1.971	3.965	
$\Lambda(1890)$	−0.080	0.291	
	Σ resonances		
	$f_{\Lambda\pi:\Sigma^\star}$	$f_{N\bar{K}:\Sigma^\star}$	
Σ	6.15	−4.76	
$\Sigma(1385)$	0	1.163	
$\Sigma(1660)$	2.09	−6.44	
$\Sigma(1670)$	0	−0.931	
$\Sigma(1750)$	0.282	0.715	

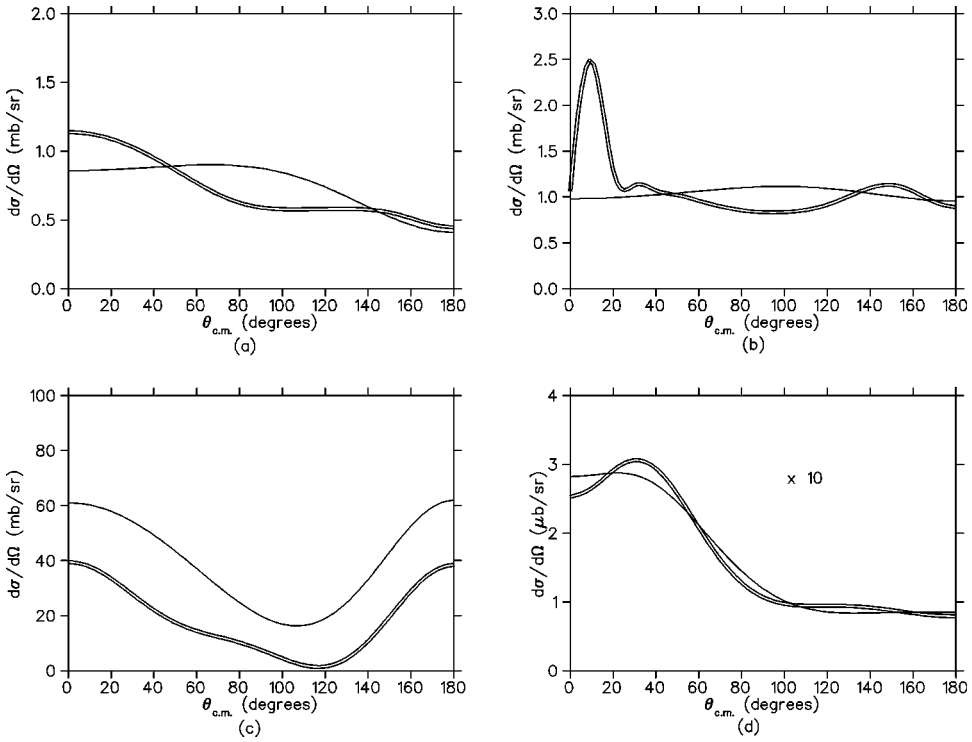

FIG. 5. Angular distributions in the c.m. for the reactions (a) K^+n elastic scattering, (b) K^+p elastic scattering, (c) $\pi^-p\rightarrow K^0\Lambda$, and (d) $\gamma p\rightarrow K^+\Lambda$. The solid curves are the calculated distributions; the double solid curves are empirical fits from Ref. [19].

$$t_{1/2^P}^{1/2,-1/2}=\sqrt{4m_B(s-m_B^2)}A_{1/2}^{1/2^P}D_{1/2\ 1/2}^{1/2}(\theta,\phi),$$

$$t_{3/2^P}^{1/2,-1/2}=\eta_P\sqrt{4m_B(s-m_B^2)}A_{1/2}^{3/2^P}D_{1/2\ 1/2}^{3/2}(\theta,\phi),$$

$$t_{3/2^P}^{3/2,1/2}=\eta_P\sqrt{4m_B(s-m_B^2)}A_{3/2}^{3/2^P}D_{3/2\ 3/2}^{3/2}(\theta,\phi). \tag{41}$$

Here the A's are the conventional photodecay amplitudes, the D's are Wigner rotation functions, and η_P is +1 or −1 for even or odd resonances. When the photon vertex functions given previously are used in these relations, one obtains

$$A_{1/2}^{1/2^P}=-\eta_P\frac{e\kappa}{2m_B}\sqrt{\frac{s-m_B^2}{2m_B}},$$

$$A_{1/2}^{3/2^P}=-\eta_P\frac{1}{4m_B}\sqrt{\frac{s-m_B^2}{m_B}}F_P(s),$$

$$A_{3/2}^{3/2^P}=-\eta_P\frac{1}{4m_B}\sqrt{\frac{s-m_B^2}{m_B}}G_P(s), \tag{42}$$

with

$$F_P(s)=\frac{1}{\sqrt{3}}\left(\frac{m_B}{\sqrt{s}}g_1+\eta_P\frac{\sqrt{s}-\eta_P m_B}{4m_B}g_2\right) \tag{43}$$

and

$$G_P(s)=g_1-\frac{\sqrt{s}-\eta_P m_B}{4m_B}g_2. \tag{44}$$

Note that these expressions are consistent with those used by Feuster and Mosel in their study of photon and meson induced reactions on the nucleon [25].

By contrast with the nonstrange resonances, there are no empirical photodecay amplitudes established for most of the strange resonances, so some other scheme is necessary for fixing the strange resonance photon couplings. One possibility is to adopt an SU(3) symmetry model which treats the electromagnetic transition operator as a U-spin scalar. This model yields relationships between the electromagnetic couplings of baryons within the same U-spin multiplet and has been used to study the magnetic moments of the ground state baryons [26]. If we suppose that the model is also valid for resonance multiplets, we obtain the relations [27]

$$\alpha_{\Lambda\Lambda^\star}=\frac{1}{2}\alpha_{nN^{\star 0}},$$

$$\alpha_{\Lambda\Sigma^{\star 0}}=-\frac{\sqrt{3}}{2}\alpha_{nN^{\star 0}} \tag{45}$$

among members of the same SU(3) octet and

$$\alpha_{\Lambda\Sigma^{\star 0}}=\frac{\sqrt{3}}{2}\alpha_{n\Delta^0} \tag{46}$$

among members of the same SU(3) decuplet, where α refers to any of the three photon couplings defined previously ($e\kappa$, g_1, or g_2). These relations allow us to extract preliminary estimates for the strange resonance photon couplings from

the couplings of nonstrange resonances within the same SU(3) octet or decuplet.

For the singlet $\Lambda(1405)$, there exists an empirical photodecay width that allows us to extract an estimate for the absolute value of the photon coupling. To find the phase of this coupling, we employ the results of the K^+ photoproduction fit of Ref. [5]. For the singlet $\Lambda(1520)$, no photon coupling is required because the kaon coupling to this resonance has been set to zero (see discussion above). Thus, this resonance cannot contribute to the photon absorption amplitude in the rescattering terms.

Unfortunately, the preliminary estimates for the resonance photon couplings proved to be quite inadequate when the cross section for reaction (24) was examined. The amplitude for this reaction has the same form as the photon absorption amplitude discussed previously. The c.m. cross section is again given by Eq. (36), except that now q_I is the 3-momentum of the incident photon, and there is an extra factor of $\frac{1}{2}$ from the average over photon polarizations.

With the original couplings, the calculated cross section for reaction (24) is much too large at intermediate and backward angles. To fix this problem, it was necessary to eliminate the photon couplings to most of those resonances not found in other fits to the proton data. These include the $N(1520)$, $N(1535)$, $\Lambda(1690)$, $\Sigma(1385)$, and $\Sigma(1750)$ resonances. We also eliminated the photon coupling to the $N(1440)$, which is either absent or small in the more recent fits. For a number of other resonances, we had to substantially modify the original photon couplings, generally in the direction of those values obtained in other fits. For example, the original signs of the $N(1710)$, $N(1720)$, and $\Sigma(1660)$ couplings were all reversed, and the coupling to the $\Lambda(1670)$, which figures prominently in several other fits, was increased by a factor of 100. We found that a number of the resonances considered, including the $N(1700)$ and the two Λ resonances above 1800 MeV, make such small contributions to the photon absorption amplitudes in the rescattering diagrams that we could disregard their photon interactions completely. Finally, it was necessary to reduce $\kappa_{\Sigma\Lambda}$ from its original value of 1.91 to a final value of 1.43.

The final values for the resonance photon couplings are listed in Table III. Note that only those resonances with nonzero couplings have been included.

Panel (d) of Fig. 5 displays the resulting cross section for reaction (24). As in the rest of this figure, the solid curve is the calculated cross section and the double solid curve the empirical cross section [19]. Note that while the fit is not perfect, the calculated cross section does reproduce the empirical cross section fairly well.

TABLE III. Photon couplings.

	Nucleon resonances					
	$e\kappa_{pN^\star+}$	$e\kappa_{nN^\star0}$	$g_1^{pN^\star+}$	$g_2^{pN^\star+}$	$g_1^{nN^\star0}$	$g_2^{nN^\star0}$
$N(1650)$	0.13	−0.036				
$N(1710)$	0.023	−0.006				
$N(1720)$			0.09	0.32	−0.20	0.14
	Δ resonances					
		$e\kappa_{N\Delta}$	$g_1^{N\Delta}$	$g_2^{N\Delta}$		
$\Delta(1620)$		0.051				
$\Delta(1232)$			1.266	1.310		
$\Delta(1600)$			0.086	0.348		
$\Delta(1700)$			−0.546	−1.087		
	Λ resonances					
			$e\kappa_{\Lambda\Lambda^\star}$			
$\Lambda(1405)$			0.018			
$\Lambda(1600)$			−0.039			
$\Lambda(1670)$			−1.32			
	Σ resonances					
		$e\kappa_{\Lambda\Sigma^\star}$	$g_1^{\Lambda\Sigma^\star}$	$g_2^{\Lambda\Sigma^\star}$		
$\Sigma(1660)$		−0.19				
$\Sigma(1670)$			0.074	−0.043		

IV. WIDTHS

The instability of the intermediate resonances can be incorporated in the model through the inclusion of widths in the resonance propagators. Only the widths of resonances excited in the s channel need to be included because for resonances excited in the u channel, the c.m. energy of the resonance is always below the threshold of the lowest decay channel. Since strange resonances cannot be excited in the s channel, the widths of these resonances need not be included. Only the widths of the nucleon and Δ resonances are required.

These widths are reasonably well known on the resonance mass shells but are generally required at positions far off the mass shells. Since the off-shell widths can be quite different from the on-shell widths, a model is needed for the energy and momentum dependence of the widths. One approach, which we adopt here, is to express the empirical widths as sums of partial widths for decay into particular channels and then to treat the energy and momentum dependence of each decay channel separately.

The decay channels open at the on-shell position of a resonance generally consist of two types: two-body channels involving a ground state baryon and a pseudoscalar meson and multibody channels involving more than two decay products. The two-body channels have already been considered in the preceding section. For those channels, the partial decay widths are given at any energy and momentum by Eqs. (34) and (35) using the couplings discussed previously. Note that at lower energies, some of the channels open at the on-shell position of a resonance will be closed, while at higher energies, additional channels can open up that are not open at the on-shell position. We will ignore these latter channels, since they are presumably important only when the width is large and the corresponding contribution to the reaction amplitude small.

The contribution of multibody channels to the on-shell width is just the difference between the empirical width and the sum of partial widths from all two-body channels. We handle these multibody channels by representing them as

TABLE IV. $N^\star$ resonance on-shell branching ratios.

Resonance	Two-body channels			Three-body channels		
	$N\pi$	$N\eta$	ΛK	$N\rho$	$N\sigma$	$\Delta(1232)\pi$
$N(1440)$	0.65			0.10		0.25
$N(1520)$	0.55			0.20	0.05	0.20
$N(1535)$	0.45	0.50		0.03	0.02	
$N(1650)$	0.75	0.06	0.06	0.08		0.05
$N(1700)$	0.10	0.017		0.063	0.22	0.60
$N(1710)$	0.15	0.01	0.15		0.26	0.43
$N(1720)$	0.15	0.012	0.07	0.768		

effective two-body channels, with the two bodies consisting of either a nucleon and a meson resonance or a pion and a baryon resonance. In particular, we include decays into the $N\rho$, $N\sigma$, $\Delta(1232)\pi$, and $N(1440)\pi$ channels. For some of these channels, there exist empirical branching ratios with large error bars [20]. After adding the corresponding widths to the two-body widths, any remaining width still not accounted for is assigned to whatever other channels are open for that resonance. Tables IV and V list the resulting on-shell branching ratios for the $N^\star$ and Δ resonances.

As for the two-body channels, we determine the off-shell structure of the multibody decay channels by choosing forms for the effective decay vertices and then evaluating the resulting widths at arbitrary energy and momenta. For the $N\sigma$ channel, which involves a scalar meson, the relevant vertex has the same form as the ground state baryon-pseudoscalar meson vertex of a resonance of opposite parity. The vertices for decays of spin $\frac{1}{2}$ resonances into the $\Delta(1232)\pi$ channel can be obtained from the vertices for decays of spin $\frac{3}{2}$ resonances into spin $\frac{1}{2}$ baryons and pseudoscalar mesons by just interchanging the initial and final baryon states. This yields the width given by Eq. (35) multiplied by a factor $2(s/m_B^2)$.

For decays of spin $\frac{3}{2}$ resonances into the $\Delta(1232)\pi$ channel or decays into the $N\rho$ channel, the vertex function involves two different couplings. The strength of only one of these couplings is fixed by the on-shell branching ratio, however, so that further input is required if both couplings are to be retained in the width calculation. To circumvent this difficulty, we resort to a minimal coupling scheme in which the general vertices are replaced by modified vertices that involve just a single coupling strength. For the $\Delta(1232)\pi$ decay channel, the modified decay vertex is obtained by keeping only the coupling of lowest order in the channel momentum. The resulting vertex then has the same form as that for decays of spin $\frac{1}{2}$ resonances into ground state baryons and pseudoscalar mesons and yields widths identical to those of Eq. (34), except for an extra factor of 5/9 in the positive parity width.

The vertex for decays of spin $\frac{1}{2}$ resonances into the $N\rho$ channel has both vector and tensor contributions. In particular, for a positive parity resonance, the vertex function is given by

$$\mathcal{V}_{\rho(1/2^+)}(p_\rho) = \left[g_V \gamma^\mu + g_T \frac{i\sigma^{\mu\nu}}{m_N}(p_\rho)_\nu \right] \epsilon_\mu, \tag{47}$$

where p_ρ and ϵ are the ρ meson 4-momentum and polarization. The negative parity vertex function has the same form but with an extra factor γ_5 to the right of the polarization vector. To obtain widths that involve a single coupling, we note that the corresponding helicity matrix elements can be expressed in terms of g_T and the coupling combination

$$F_P(s) = g_V + g_T \frac{\sqrt{s} + \eta_P m_N}{2m_N}, \tag{48}$$

where the index P specifies the resonance parity. If just the F_P terms are retained in the matrix elements, the center of mass width reduces to

$$\Gamma\left(\frac{1}{2}^P \to \frac{1}{2}^+ + 1^-\right) = \frac{F_P^2}{4\pi m_\rho^2} \frac{p_\rho^3 E_P}{\sqrt{s}} \left[\left(1 - \frac{E_\rho}{E_P}\right)^2 + 2\left(\frac{m_\rho}{E_P}\right)^2 \right] \tag{49}$$

with

$$E_P = E_N + \eta_P m_N. \tag{50}$$

We employ this expression with F_P evaluated at the on-shell point, $s = m_R^2$.

For decays of spin $\frac{3}{2}$ resonances into the $N\rho$ channel, the decay vertex has the same form as the corresponding photon vertex defined previously. To obtain widths with just a single coupling for these decays, we simply drop the terms involving g_2. This yields the center of mass width

TABLE V. Δ resonance on-shell branching ratios.

Resonance	Two-body channels		Three-body channels	
	$N\pi$	$N\rho$	$\Delta(1232)\pi$	$N(1440)\pi$
$\Delta(1232)$	1.0			
$\Delta(1600)$	0.17	0.08	0.55	0.20
$\Delta(1620)$	0.25	0.20	0.55	
$\Delta(1700)$	0.15	0.40	0.45	

$$\Gamma\left(\frac{3^P}{2}\rightarrow\frac{1^+}{2}+1^-\right)=\left(\frac{g_1}{2m_N}\right)^2\frac{1}{8\pi}\frac{p_\rho^3 E_P}{3\sqrt{s}}\left[\left(1-\frac{E_\rho}{E_P}\right)^2+2\left(\frac{E_\rho^2+p_\rho^2}{E_P m_\rho}\right)^2+3\left(1+\frac{E_\rho}{E_P}\right)^2\right]. \tag{51}$$

The model employed to represent multibody decay channels involves unstable decay products, in particular, the ρ meson in the $N\rho$ channel and the baryon resonances in the $\Delta(1232)\pi$ and $N(1440)\pi$ channels. In each such channel, the decay amplitude is spread out over a range of masses determined by the width of the unstable decay product. To take this mass spread into account, we replace the width expressions discussed earlier with expressions of the form

$$\Gamma(s)=\frac{g^2}{4\pi}\int_{m_{min}}^{m_{max}}\mathcal{P}(s,x)\mathcal{S}(x)dx, \tag{52}$$

where g is the coupling strength, and the phase space factor $\mathcal{P}$ is obtained by replacing the unstable decay product mass in the appropriate width formula with the integration variable x. The integration limits are defined by

$$m_{min}=\sqrt{s_{thr}}-m_{stable},$$

$$m_{max}=\sqrt{s}-m_{stable}, \tag{53}$$

where m_{stable} is the mass of the stable decay product (m_N for ρ meson decays and m_π for decays to unstable baryon resonances) and $\sqrt{s_{thr}}$ is the minimum center of mass energy required to form the unstable decay product in its dominant production mode. This latter quantity is just equal to m_N+m_π for the $\Delta(1232)$ and $N(1440)$ resonances and $m_\pi+m_\pi$ for the ρ meson.

For the strength distribution function, we employ the Breit-Wigner form

$$\mathcal{S}(x)=\frac{A}{2\pi}\frac{\Gamma_{pr}}{(x-m_C)^2+\frac{1}{4}\Gamma_{pr}^2}, \tag{54}$$

where Γ_{pr} is the empirical width of the unstable decay product and m_C is the center of its mass distribution. The normalization factor A is defined by the requirement that

$$\int_{m_{min}}^{\infty}\mathcal{S}(x)dx=1, \tag{55}$$

which yields

$$\frac{1}{A}=\frac{1}{2}+\frac{1}{\pi}\arctan\left(\frac{m_C-x_{min}}{\Gamma_{pr}}\right). \tag{56}$$

V. MATRIX ELEMENTS

To obtain the photoproduction cross section, the matrix elements of the reaction amplitude must be evaluated between an initial deuteron state and the final Λn state. This is most readily accomplished in momentum space in the deuteron rest frame. In any other frame of reference, the numerical evaluation of the rescattering matrix elements is substantially more difficult.

As discussed in the Introduction, we employ a nonrelativistic deuteron wave function to represent the initial state and omit all interactions from the final state. The final state is then just a product of free Dirac spinors representing the two outgoing baryons.

The initial state can be expressed as a product of an isospin factor and a spin-spatial wave function,

$$\Psi_M(\mathbf{p})=|(pn)I=0\rangle\Phi_M(\mathbf{p}), \tag{57}$$

where M and $\mathbf{p}$ are the deuteron spin projection and relative 3-momentum, and

$$|(pn)I=0\rangle=\frac{1}{\sqrt{2}}(|pn\rangle-|np\rangle). \tag{58}$$

As mentioned previously, the inverse $\sqrt{2}$ above and the factor 2 associated with the diagrams not shown in Figs. 1 and 2 are taken into account by including an extra factor $\sqrt{2}$ in the matrix elements. The minus sign in Eq. (58) is accounted for by including an extra minus sign in the neutral meson exchange contributions to the rescattering amplitudes. The function Φ can be further decomposed into products of spin and spatial wave functions,

$$\Phi(\mathbf{p})=\sum_{M_S}\psi_{M,M_S}(\mathbf{p})|1M_S\rangle \tag{59}$$

with

$$|1M_S\rangle=\sum_{M_p,M_n}\left(\frac{1}{2}M_p\frac{1}{2}M_n|1M_S\right)\chi_{M_p}\chi_{M_n} \tag{60}$$

and

$$\psi_{M,M_S}(\mathbf{p})=\sum_{L=0,2}(LM-M_S1M_S|1M)\tilde{\phi}_L(p)Y_{LM-M_S}(\theta_p,\phi_p), \tag{61}$$

where

$$\tilde{\phi}_L(p)=\sqrt{\frac{2}{\pi}}i^L\int_0^\infty r^2\phi_L(r)j_L(pr)dr \tag{62}$$

is the radial part of the deuteron wave function in momentum space.

In terms of these initial and final states, the photoproduction matrix elements have the form

$$\langle F|\hat{T}|I\rangle=\sqrt{(2\pi)^3 2m_d}(\mathcal{M}^{ia}_{M_\Lambda M_{nF}M}+\mathcal{M}^{rs}_{M_\Lambda M_{nF}M}), \tag{63}$$

where M_Λ and M_{nF} are the spin projections of the outgoing Λ and neutron, and the factor containing the deuteron mass m_d is a normalization factor. In the impulse term, the 4-momentum of the spectator neutron is fixed by energy-momentum conservation, and the initial and final neutron spin projections must be equal. Hence, the first term in Eq. (63) can be written as

$$\mathcal{M}^{ia}_{M_\Lambda M_{nF} M} = \mathcal{T}^{ia}_{M_\Lambda M_{nF} M}(\mathbf{p}) = \sum_{M_S} \psi_{M,M_S}(\mathbf{p}) \times \left(\frac{1}{2} M_S - M_{nF} \frac{1}{2} M_{nF} | 1 M_S \right) t^{ia}_{M_\Lambda M_{nF} M_S - M_{nF} M_{nF}}, \tag{64}$$

with $\mathbf{p} = -\mathbf{p}_{nF}$, $p^0 = \frac{1}{2} m_d - E_{nF}$, and

$$t^{ia}_{M_\Lambda M_{nF} M_S - M_{nF} M_{nF}} = \overline{u}_{M_\Lambda}(p_\Lambda) \hat{T}_{ia} u_{M_S - M_{nF}}(p_p) \delta(p_{nF} - p_{nI}), \tag{65}$$

where $\hat{T}_{ia}$ is the sum of impulse amplitudes defined in Sec. II.

The relative deuteron 4-momentum is not fixed in the second term, however, so that, in principle, a four-dimensional loop integration is required to evaluate the rescattering matrix element. Since we wish to employ a nonrelativistic deuteron wave function, some prescription is needed to fix the energy variable in this integration. The four-dimensional integration then reduces to a three-dimensional integration over the deuteron relative momentum. For most of the results reported in the following section, we have fixed the energy variable in the loop integration by requiring that the deuteron energy be equally shared by the proton and neutron. We have attempted to check the sensitivity of our results to this choice by performing additional calculations with an arbitrary energy added to the incident nucleon attached to the photon absorption line and the same energy subtracted from the nucleon attached to the kaon emission line (so that the total deuteron energy is unchanged).

With the relative deuteron energy fixed, the second term in Eq. (63) can be written as

$$\mathcal{M}^{rs}_{M_\Lambda M_{nF} M} = \int \frac{d^3 p}{(2\pi)^{3/2}} \mathcal{T}^{rs}_{M_\Lambda M_{nF} M}(\mathbf{p}), \tag{66}$$

where $\mathcal{T}^{rs}$ is defined by an equation analogous to Eq. (64) with

$$t^{rs}_{M_\Lambda M_{nF} M_p M_{nI}} = \overline{u}_{M_\Lambda}(p_\Lambda) \overline{u}_{M_{nF}}(p_{nF}) \hat{T}_{rs} u_{M_{nI}}(p_{nI}) u_{M_p}(p_p). \tag{67}$$

The various contributions to this quantity represented by the diagrams in Fig. 2 can all be expressed as products of a photon absorption matrix element, a meson propagator, and a kaon emission matrix element. The charged pion exchange contribution from diagram (a), for example, has the form

$$t^{A,\pi^+}_{M_\Lambda M_{nF} M_p M_{nI}} = \overline{u}_{M_{nF}}(p_{nF}) \hat{T}_\gamma u_{M_p}(p_p) G_\pi(q) \overline{u}_{M_\Lambda}(p_\Lambda) \hat{T}_K u_{M_{nI}}(p_{nI}). \tag{68}$$

The two-body matrix elements appearing in Eq. (68), as well as those associated with other rescattering terms, have the general structure

$$\overline{u}_{M_F}(p_F) \hat{T} u_{M_I}(p_I) = \overline{u}_{M_F}(p_F) [\hat{A} + \hat{B} \gamma_5 + \hat{C} \gamma^0 + \hat{D} \gamma^0 \gamma_5] u_{M_I}(p_I), \tag{69}$$

where the operators $\hat{A}$, $\hat{B}$, $\hat{C}$, and $\hat{D}$ depend upon the amplitude considered and the spin and parity of the resonance involved. Detailed expressions for these operators are given in the Appendix. Carrying out the Dirac algebra in Eq. (69) yields the equivalent Pauli form

$$\overline{u}_{M_F}(p_F) \hat{T} u_{M_I}(p_I) = N_F N_I \chi^\dagger_{M_F} [(\hat{A} + \hat{C}) + (\hat{B} + \hat{D}) \sigma \cdot \hat{p}_I + \sigma \cdot \hat{p}_F (\hat{D} - \hat{B}) + \sigma \cdot \hat{p}_F (\hat{C} - \hat{A}) \sigma \cdot \hat{p}_I] \chi_{M_I} \tag{70}$$

with

$$N = \sqrt{\frac{E + m}{2m}} \tag{71}$$

and

$$\hat{p} = \frac{\mathbf{p}}{E + m}. \tag{72}$$

This last expression can be further reduced analytically, but the procedure is extremely tedious, especially for the rescattering terms. Instead, we evaluate the Pauli matrix elements numerically.

An alternative procedure is to evaluate the two-body Dirac matrix elements directly without resorting to the decomposition given by Eq. (69). We have written separate numerical codes to evaluate the matrix elements by both methods. Agreement in the results not only confirms the accuracy of the codes themselves, but also provides a check of the algebraic results given in the Appendix.

The angle integrals in Eq. (66) are carried out using a two-dimensional Gauss points technique. Without form factors, the radial integrals diverge, due both to the momentum dependence associated with the lower components of the incident Dirac spinors [Eq. (70)] and to the momentum dependence in the spin $\frac{3}{2}$ propagators [Eq. (18)] and photon vertices [Eq. (20)]. The radial integrals are further complicated by pole singularities associated with the meson propagator. In the NN interaction, such poles generate the imaginary part of the t matrix from a real K matrix and are usually treated analytically. Here, however, the pole positions are angle dependent due to the choice of integration variable in the loop integrals and cannot be easily handled analytically.

To make the radial integrals converge, we introduce form factors at the internal meson-baryon vertices. Physically, these form factors are supposed to take account of the internal structure of the mesons and baryons participating in the interaction. Instead of the usual dipole form factors, whose incorporation would introduce additional nonphysical poles into the radial integrand, we employ the exponential form

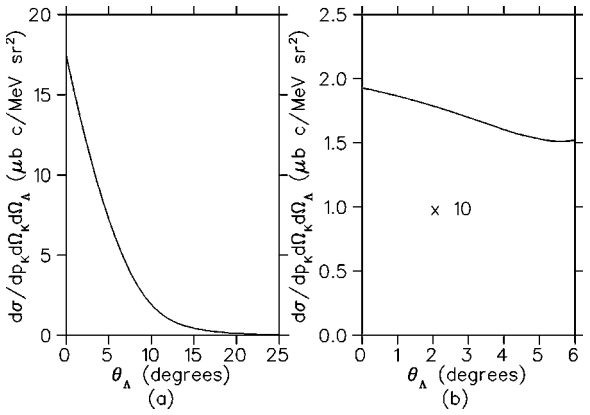

FIG. 6. Impulse contribution to the differential cross section for (a) E_γ=1230 MeV, T_K=500 MeV, and θ_K=10°; and (b) E_γ =1367 MeV, T_K=620 MeV, and θ_K=20°.

$$F(q) = \exp\left(-\frac{|q^2 - m_M^2|}{2\Lambda_M^2}\right), \tag{73}$$

where m_M and q are the mass and 4-momentum of the exchanged meson, and Λ_M is a scale factor. Two such factors are included, one at each internal meson-baryon vertex. Most of the results presented in the following section have been obtained with the choice Λ=1500 MeV for all exchanged mesons. However, we have also obtained results with other values of Λ to check the sensitivity of our results to the form factor scale.

To handle the meson pole singularities, we introduce a small imaginary parameter in the meson propagators and then numerically evaluate the radial integrals as this parameter is made to approach zero. We have checked that this procedure converges well and that it yields the correct result for a test integral that can be evaluated analytically. Because radial pole singularities can occur at quite large momentum values, depending on the angle of the deuteron relative momentum vector, it is necessary to carry out the radial integrals to several GeV/c to ensure convergence, even when exponential form factors are incorporated. Nevertheless, the insensitivity of the results to the form factor scale, within a reasonable range for this scale, indicates that the bulk of the calculated cross sections is associated with rather modest values of the deuteron relative momentum.

VI. NUMERICAL RESULTS AND DISCUSSION

In this section we present results for the differential photoproduction cross section in the deuteron rest frame,

$$\frac{d^5\sigma}{dp_K d\Omega_K d\Omega_\Lambda} = \frac{1}{12}\frac{1}{(2\pi)^2}\frac{m_\Lambda m_n p_\Lambda p_K^2}{E_B E_K E_\gamma}\gamma(\theta_\Lambda)\sum_{spins}|\langle F|\hat{T}|I\rangle|^2, \tag{74}$$

where

$$\gamma^{-1} = \left[1 - \frac{E_\Lambda P_B}{E_B p_\Lambda}\cos(\theta_\Lambda)\right]. \tag{75}$$

Here E_B and $\mathbf{P_B}$ are the total outgoing baryon energy and 3-momentum in the deuteron rest frame, and θ_Λ is the angle between the Λ momentum and $\mathbf{P_B}$. The expression is evaluated using a coordinate system with the z axis along the incident photon direction and the kaon momentum in the xz plane with $p_{Kx} > 0$.

The differential cross section given above depends on five independent kinematic variables. We have chosen the inci-

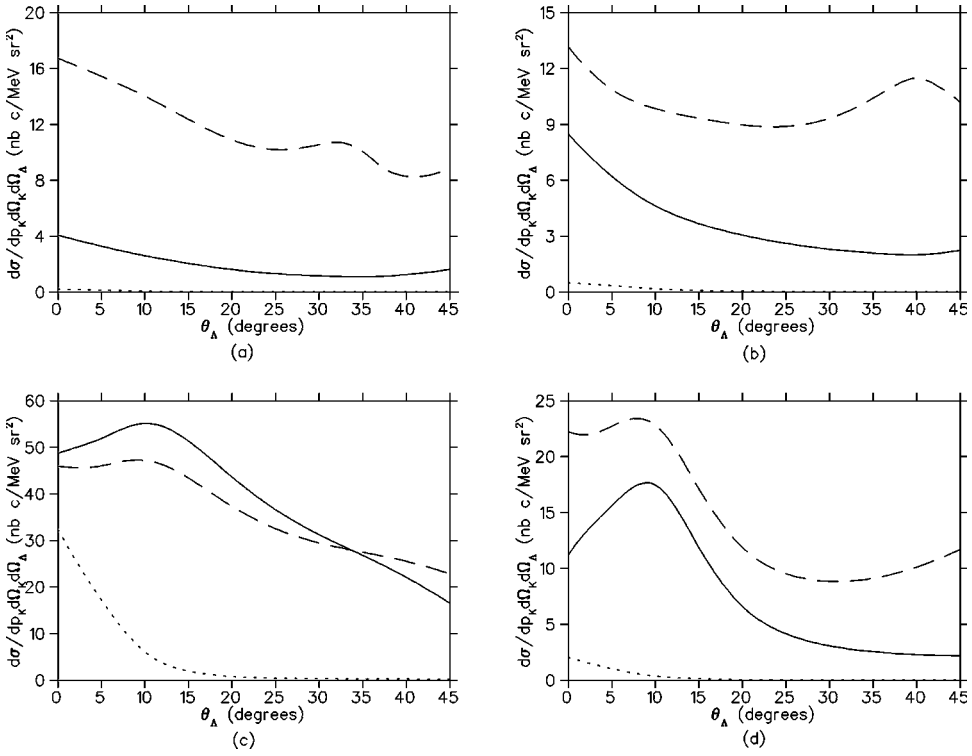

FIG. 7. Differential cross sections for E_γ=1500 MeV and various choices for T_K and θ_K: (a) T_K=200 MeV and θ_K=15°, (b) T_K=300 MeV and θ_K=15°, (c) T_K=500 MeV and θ_K=15°, and (d) T_K=300 MeV and θ_K=30°. The solid and dashed curves were obtained with the rescattering models A and B discussed in the text plus impulse terms; the dotted curves were obtained with impulse terms only.

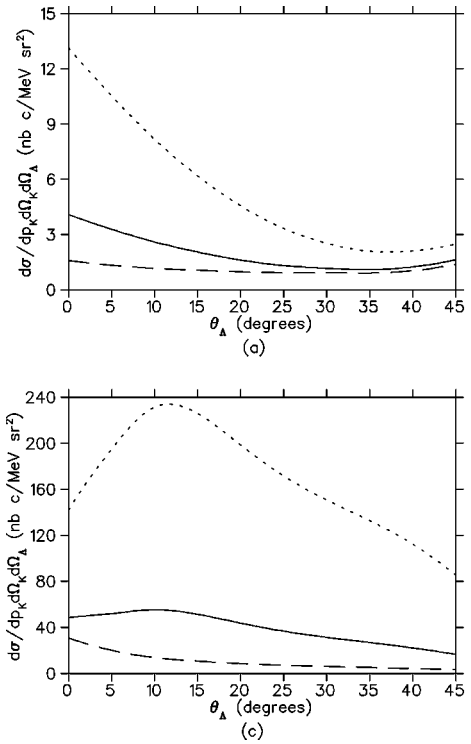

FIG. 8. Differential cross sections for $E_\gamma = 1500$ MeV, $\theta_K = 15°$, and various choices for T_K: (a) $T_K = 200$ MeV, (b) $T_K = 300$ MeV, and (c) $T_K = 500$ MeV. The dashed curves were obtained with $\Lambda = 1200$ MeV, the solid curves with $\Lambda = 1500$ MeV, and the dotted curves with $\Lambda = 1800$ MeV.

dent photon energy E_γ, the kaon kinetic energy T_K, the kaon angle θ_K defined relative to the incident photon direction, the Λ angle θ_Λ defined above, and the angle ϕ between the plane containing p_Λ and p_n and the plane containing p_γ and p_K (the xz plane). In all figures displayed here, ϕ has been set to zero and the cross section plotted as a function of θ_Λ for fixed values of the other three parameters. Calculations carried out with other values for ϕ indicate that the cross section does not depend significantly on this parameter.

In the absence of final state correlations, the strength of the impulse term is determined primarily by the strength of the deuteron wave function and thus depends mainly on the spectator neutron momentum. When this momentum is small, the cross section is dominated by the impulse term. In Fig. 6, we present results for two kinematical situations where this is the case. The cross sections displayed here have been obtained with just the impulse terms and are several times larger than those of Li and Wright [16], which also

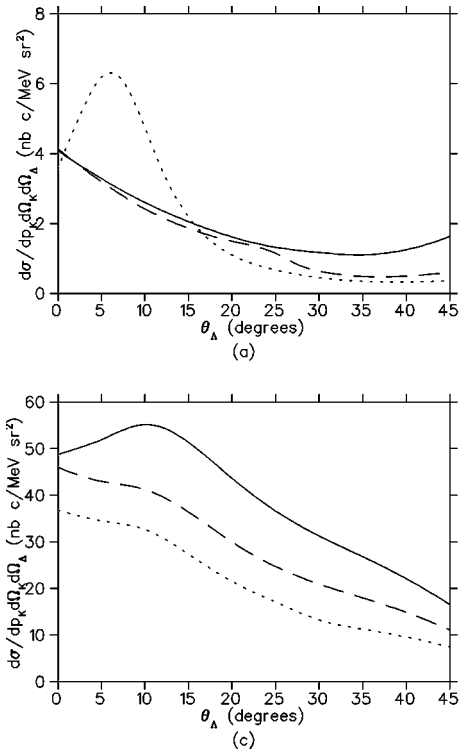

FIG. 9. Differential cross sections for the same kinematics as in Fig. 8. The solid curves were obtained with a deuteron energy increment of 0 MeV, the dashed curves with an energy increment of 100 MeV, and the dotted curves with an energy increment of 200 MeV, as explained in the text.

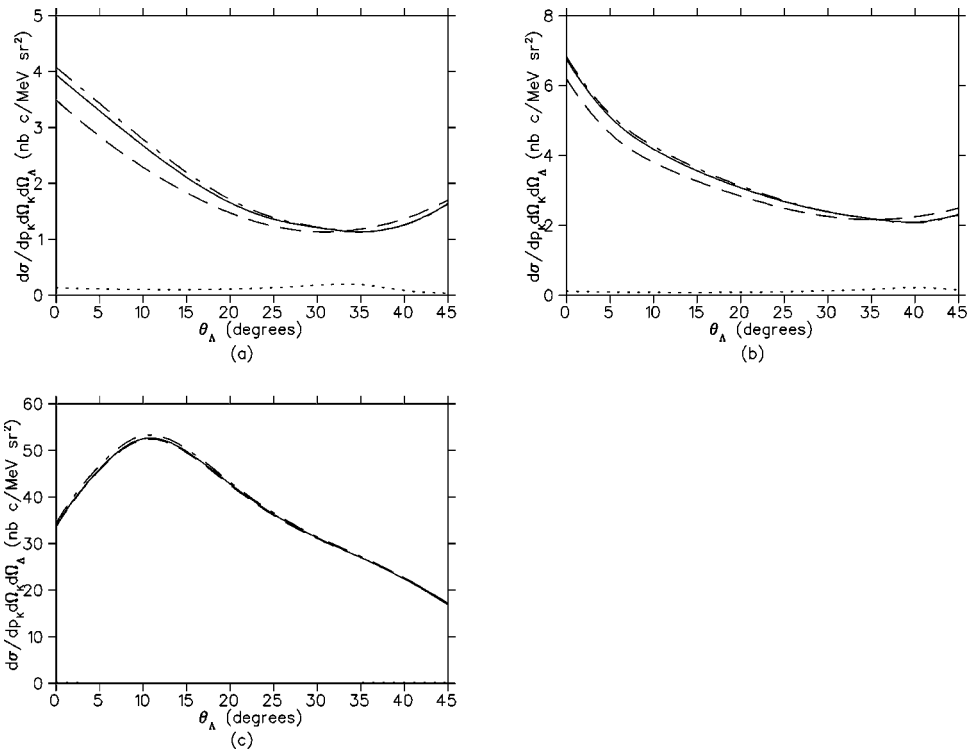

FIG. 10. Rescattering contributions to the differential cross section for the same kinematics as in Fig. 8. The solid curves were obtained with the full rescattering model, the dashed curves with just the pion exchange rescattering terms included, the dotted curves with just the kaon exchange rescattering terms included, and the dot-dashed curves with the pion and kaon exchange rescattering terms included.

include just the impulse terms. Our coupling strengths are rather different from theirs, and we have employed a different deuteron wave function and different forms for the spin $\frac{3}{2}$ propagators and vertices. All of these differences influence the calculated results, but it is rather surprising that our cross sections differ so much from theirs.

More recent results based on the impulse approximation have also been reported in Ref. [17]. However, these later results are not given in the deuteron rest frame, which we have employed in our calculations to facilitate the evaluation of the rescattering terms, so no direct comparison with our results is possible. It should be emphasized that we are primarily interested here in kinematical regimes where the impulse contribution is small and which have not been examined in previous analyses.

When the neutron spectator momentum exceeds a few tens of MeV/c, the impulse strength drops dramatically, and the photoproduction matrix elements are dominated by the rescattering contributions. This is illustrated in Fig. 7 where the differential cross section is plotted against θ_Λ for $E_\gamma = 1500$ MeV and various choices for T_K and θ_K. The solid and dashed curves in this figure represent results obtained with two different rescattering models. In model A (solid curves), intermediate baryon lines in the rescattering diagrams include only resonance states. In model B (dashed curves), ground state baryons are included as intermediate baryon states in the crossed (u-channel) amplitudes but not in the direct (s-channel) amplitudes. In the direct amplitudes the absence of nucleon widths would lead to poles in the nucleon propagators, were nucleons to be included in the intermediate states. These poles are difficult to handle numerically. These poles do not occur in the s-channel impulse term, and thus intermediate baryon states are included in all the impulse terms in both models.

The curves in Fig. 7 reveal that the rescattering amplitudes are substantially larger than the impulse amplitudes in a variety of kinematic situations. The results displayed also indicate that the results obtained with the two rescattering models can be significantly different. This result warrants further study. The remaining figures, which explore the dependence of the calculated results on various dynamical features of the model, have all been obtained with model A.

Figure 8 displays the dependence of the calculated cross sections on the form factors discussed in the preceding section. As seen in the figures, the cross sections depend moderately on the form factor mass when this mass is below our standard choice of 1500 MeV. For masses above 1500 MeV, however, the form factor dependence becomes quite strong. This suggests that the rescattering contributions receive most of their strength from low or moderate values of the deuteron relative momentum and gives us some confidence that our form factor prescription is not unreasonable.

As mentioned in Sec. V, the four-dimensional loop integral is reduced to a three-dimensional integral by arbitrarily assigning half the deuteron energy to the proton and half to the neutron. We have attempted to determine the sensitivity

of the calculated cross sections to this prescription by defining a deuteron energy increment ΔE through the relations

$$E_{N\gamma} = \frac{1}{2}E_d + \Delta E,$$

$$E_{NK} = \frac{1}{2}E_d - \Delta E, \tag{76}$$

where $E_{N\gamma}$ is the energy of the incident nucleon on the photon absorption line and E_{NK} is the energy of the incident nucleon on the kaon emission line, and carrying out calculations with several values for this increment. The results are exhibited in Fig. 9. The sensitivity to ΔE revealed here suggests that a better treatment of the deuteron relative energy would be desirable; however, the sensitivity is not so large as to invalidate the conclusions derived from our results.

Contributions to the rescattering terms from different meson exchanges are compared in Fig. 10. The solid curves displayed here were obtained with all three meson exchanges—π, K, and η—included in the rescattering contributions, but with the impulse terms suppressed. The remaining curves were obtained with different combinations of π and K exchange, as specified in the figure caption. A comparison of the curves in each panel reveals that the π exchange terms are by far the most important, but that at smaller values of T_K, kaon exchange terms make non-negligible contributions as well.

A possible source of uncertainty in our results that we have not explored lies in the neglect of off-shell terms in the spin $\frac{3}{2}$ propagator and the spin $\frac{3}{2}$ electromagnetic vertex. Although these terms do not affect kaon photoproduction from the proton very dramatically [12], they could be quite important in the rescattering terms here, where the intermediate resonances are generally far off-shell. Certainly, a thorough investigation of the off-shell terms would be desirable in any future study.

In summary, we have examined kaon photoproduction from the deuteron within a fairly elaborate model that includes meson rescattering terms. Our results indicate that the rescattering contributions to the amplitude may be significant over a wide kinematical range. Only when the spectator neutron momentum is small is the cross section dominated by the impulse contribution.

Several improvements in the model could be made. To remove the arbitrariness introduced in the evaluation of the rescattering loop integrals, a more rigorous treatment of the deuteron relative energy is required. Some means must also be found for incorporating off-shell terms into the treatment of the $\frac{3}{2}$ resonances. Finally, although the model includes vector meson exchange in a very approximate way through the use of pseudoscalar meson form factors, it would be better to include vector meson exchanges explicitly.

APPENDIX: AMPLITUDE OPERATORS

The operators defined by Eq. (69) in Sec. V depend upon the amplitude considered and the spin and parity of the resonance involved. For positive parity spin $\frac{1}{2}$ resonances, the kaon emission operators are given by

$$\hat{A}^K_{1/2^+} = -G_K(s)m_R,$$

$$\hat{B}^K_{1/2^+} = 0,$$

$$\hat{C}^K_{1/2^+} = G_K(s)E_R,$$

$$\hat{D}^K_{1/2^+} = -G_K(s)\sigma\cdot\mathbf{p}_R \tag{A1}$$

with

$$G_K(s) = g_K g_M D(s), \tag{A2}$$

where g_K and g_M are the couplings at the kaon emission and meson absorption vertices, and

$$D(s) = (s - m_R^2 + i m_R\Gamma_R)^{-1}. \tag{A3}$$

The corresponding photon absorption operators are

$$\hat{A}^{\gamma d}_{1/2^+} = G_\gamma(s)m_R\Omega(p_\gamma,\epsilon),$$

$$\hat{B}^{\gamma d}_{1/2^+} = G_\gamma(s)m_R\Sigma(p_\gamma,\epsilon),$$

$$\hat{C}^{\gamma d}_{1/2^+} = -G_\gamma(s)\Omega_3(p_R,p_\gamma,\epsilon),$$

$$\hat{D}^{\gamma d}_{1/2^+} = -G_\gamma(s)\Sigma_3(p_R,p_\gamma,\epsilon) \tag{A4}$$

for the s-channel impulse term and rescattering diagrams (a), (b), and (c) and

$$\hat{A}^{\gamma c}_{1/2^+} = G_\gamma(s)m_R\Omega(p_\gamma,\epsilon),$$

$$\hat{B}^{\gamma c}_{1/2^+} = G_\gamma(s)m_R\Sigma(p_\gamma,\epsilon),$$

$$\hat{C}^{\gamma c}_{1/2^+} = G_\gamma(s)\Omega_3(p_\gamma,\epsilon,p_R),$$

$$\hat{D}^{\gamma c}_{1/2^+} = G_\gamma(s)\Sigma_3(p_\gamma,\epsilon,p_R) \tag{A5}$$

for the u-channel impulse term and rescattering diagrams (d), (e), and (f) with

$$G_\gamma(s) = g_\gamma g_M D(s). \tag{A6}$$

The Σ and Ω operators here are defined by the relations

$$\Sigma(a,b) = a_0 b_0 - \sigma\cdot\mathbf{a}\sigma\cdot\mathbf{b},$$

$$\Omega(a,b) = b_0\sigma\cdot\mathbf{a} - a_0\sigma\cdot\mathbf{b}, \tag{A7}$$

and

$$\Sigma_3(a,b,c) = a_0\Sigma(b,c) - \sigma\cdot\mathbf{a}\Omega(b,c),$$

$$\Omega_3(a,b,c) = a_0\Omega(b,c) - \sigma\cdot\mathbf{a}\Sigma(b,c), \tag{A8}$$

where a_0 and $\mathbf{a}$ are the time and space components of the 4-vector a.

For $\frac{3}{2}^+$ resonances, the kaon emission operators take the form

$$\hat{A}^{Kd}_{3/2^+} = \tilde{G}_K(s)\left[m_R Q + \Sigma(p_R,h) - \frac{m_R}{3}\Sigma(p_K,p_M)\right],$$

$$\hat{B}^{Kd}_{3/2^+} = \tilde{G}_K(s)\left[\Omega(p_R,h) - \frac{m_R}{3}\Omega(p_K,p_M)\right],$$

$$\hat{C}^{Kd}_{3/2^+} = \tilde{G}_K(s)\left[E_R Q + m_R h_0 - \frac{1}{3}\Sigma_3(p_R,p_K,p_M)\right],$$

$$\hat{D}^{Kd}_{3/2^+} = \tilde{G}_K(s)\left[- Q\sigma\cdot\mathbf{p}_R - m_R\sigma\cdot\mathbf{h} - \frac{1}{3}\Omega_3(p_R,p_K,p_M)\right] \tag{A9}$$

for diagrams (a) and (c) and

$$\hat{A}^{Kc}_{3/2^+} = \tilde{G}_K(s)\left[m_R Q - \Sigma(p_R,h) - \frac{m_R}{3}\Sigma(p_M,p_K)\right],$$

$$\hat{B}^{Kc}_{3/2^+} = \tilde{G}_K(s)\left[- \Omega(p_R,h) - \frac{m_R}{3}\Omega(p_M,p_K)\right],$$

$$\hat{C}^{Kc}_{3/2^+} = \tilde{G}_K(s)\left[E_R Q - m_R h_0 - \frac{1}{3}\Sigma_3(p_R,p_M,p_K)\right],$$

$$\hat{D}^{Kc}_{3/2^+} = \tilde{G}_K(s)\left[- Q\sigma\cdot\mathbf{p}_R + m_R\sigma\cdot\mathbf{h} - \frac{1}{3}\Omega_3(p_R,p_M,p_K)\right] \tag{A10}$$

for the remaining rescattering diagrams with

$$\tilde{G}_K(s) = \frac{G_K(s)}{m_\pi^2}, \tag{A11}$$

$$Q = p_K\cdot p_M - \frac{2}{3m_R^2}(p_K\cdot p_R)(p_M\cdot p_R), \tag{A12}$$

and

$$h = \frac{1}{3m_R}[(p_K\cdot p_R)p_M - (p_M\cdot p_R)p_K], \tag{A13}$$

where p_M and p_K are the 4-momenta of the absorbed meson and emitted kaon.

To specify the $\frac{3}{2}^+$ photon absorptions operators, we define the coupling constant combinations

$$\beta_1 = F_1 + F_2,$$

$$\beta_2 = F_2 - 2F_1,$$

$$\beta_3 = 3F_1 - F_2 \tag{A14}$$

with

$$F_1 = \frac{g_M}{m_\pi}\frac{g_1}{2m_B}D(s),$$

$$F_2 = \frac{g_M}{m_\pi}\frac{m_R g_2}{4m_B^2}D(s), \tag{A15}$$

where m_B is the mass of the ground state baryon at the photon vertex. In terms of these couplings,

$$\hat{A}^{\gamma d}_{3/2^+} = \frac{1}{3}[\beta_1\Omega(p_M,k_R) + 2F_1(p_M\cdot p_R)\Omega(p_\gamma,\epsilon) - 3\Omega(p_R,q_1) - 2F_1\Omega_4(p_R,p_M,p_\gamma,\epsilon)],$$

$$\hat{B}^{\gamma d}_{3/2^+} = \frac{1}{3}[\beta_1\Sigma(p_M,k_R) + 2F_1(p_M\cdot p_R)\Sigma(p_\gamma,\epsilon) - 3\Sigma(p_R,q_1) - 2F_1\Sigma_4(p_R,p_M,p_\gamma,\epsilon) - 3F_2(p_M\cdot k_R)],$$

$$\hat{C}^{\gamma d}_{3/2^+} = \frac{1}{3m_R}[\beta_1\Omega_3(p_R,p_M,k_R) + 2F_1(p_M\cdot p_R)\Omega_3(p_R,p_\gamma,\epsilon) + 3F_2(p_M\cdot k_R)\sigma\cdot\mathbf{p}_R + 3m_R^2\sigma\cdot\mathbf{q}_1 - 2m_R^2F_1\Omega_3(p_M,p_\gamma,\epsilon)],$$

$$\hat{D}^{\gamma d}_{3/2^+} = \frac{1}{3m_R}[\beta_1\Sigma_3(p_R,p_M,k_R) + 2F_1(p_M\cdot p_R)\Sigma_3(p_R,p_\gamma,\epsilon) - 3F_2(p_M\cdot k_R)E_R - 3m_R^2q_1^0 - 2m_R^2F_1\Sigma_3(p_M,p_\gamma,\epsilon)] \tag{A16}$$

for the s-channel impulse term and rescattering diagrams (a), (b), and (c) and

$$\hat{A}^{\gamma c}_{3/2^+} = \frac{1}{3}[-\beta_3\Omega(k_R,p_M) - 2F_1(p_M\cdot p_R)\Omega(\epsilon,p_\gamma) + 3\Omega(p_R,q_1) + 2F_1\Omega_4(p_R,\epsilon,p_\gamma,p_M)],$$

$$\hat{B}^{\gamma c}_{3/2^+} = \frac{1}{3}[-\beta_3\Sigma(k_R,p_M) - 2F_1(p_M\cdot p_R)\Sigma(\epsilon,p_\gamma) + 3\Sigma(p_R,q_1) + 2F_1\Sigma_4(p_R,\epsilon,p_\gamma,p_M) - 3\beta_2(p_M\cdot k_R)],$$

$$\hat{C}^{\gamma c}_{3/2^+} = \frac{1}{3m_R}[-\beta_1\Omega_3(p_R,k_R,p_M) - 2F_1(p_M\cdot p_R)\Omega_3(p_R,\epsilon,p_\gamma) - 3F_2(p_M\cdot k_R)\sigma\cdot\mathbf{p}_R - 3m_R^2\sigma\cdot\mathbf{q}_2 + 2m_R^2F_1\Omega_3(\epsilon,p_\gamma,p_M)],$$

$$\hat{D}^{\gamma c}_{3/2^+} = \frac{1}{3m_R}[-\beta_1\Sigma_3(p_R,k_R,p_M) - 2F_1(p_M\cdot p_R)\Sigma_3(p_R,\epsilon,p_\gamma) + 3F_2(p_M\cdot k_R)E_R + 3m_R^2q_2^0 + 2m_R^2F_1\Sigma_3(\epsilon,p_\gamma,p_M)] \tag{A17}$$

for the u-channel impulse term and rescattering diagrams (d), (e), and (f), where

$$q_1 = F_1 k_M + \beta_2 \frac{p_M \cdot p_R}{3m_R^2} k_R,$$

$$q_2 = F_1 k_M - F_2 \frac{p_M \cdot p_R}{3m_R^2} k_R \tag{A18}$$

with

$$k_M = (p_M \cdot \epsilon) p_\gamma - (p_M \cdot p_\gamma)\epsilon,$$

$$k_R = (p_R \cdot \epsilon) p_\gamma - (p_R \cdot p_\gamma)\epsilon. \tag{A19}$$

The Σ_4 and Ω_4 operators in these expressions are defined by

$$\Sigma_4(a,b,c,d) = \Sigma(a,b)\Sigma(c,d) + \Omega(a,b)\Omega(c,d),$$

$$\Omega_4(a,b,c,d) = \Sigma(a,b)\Omega(c,d) + \Omega(a,b)\Sigma(c,d). \tag{A20}$$

The negative parity operators are given by the same expressions as these except for extra minus signs multiplying the $\hat{A}$ and $\hat{B}$ kaon emission operators and the $\hat{C}$ and $\hat{D}$ photon absorption operators.

Finally, for the t-channel impulse terms, we define the combinations

$$\alpha^V_{K^\star} = \frac{g_{\gamma KK^\star}}{m_{sc}} g^V_{p\Lambda K^\star} \frac{1}{p^2_{K^\star} - m^2_{K^\star} + i m_{K^\star}\Gamma_{K^\star}},$$

$$\alpha^T_{K^\star} = \frac{g_{\gamma KK^\star}}{m_{sc}} \frac{g^T_{p\Lambda K^\star}}{m_\Lambda + m_p} \frac{1}{p^2_{K^\star} - m^2_{K^\star} + i m_{K^\star}\Gamma_{K^\star}} \tag{A21}$$

for the $K^\star(892)$ resonance and

$$\alpha^V_{K1} = \frac{g_{\gamma KK1}}{m_{sc}} g^V_{p\Lambda K1} \frac{1}{p^2_{K1} - m^2_{K1} + i m_{K1}\Gamma_{K1}},$$

$$\alpha^T_{K1} = \frac{g_{\gamma KK1}}{m_{sc}} \frac{g^T_{p\Lambda K1}}{m_\Lambda + m_p} \frac{1}{p^2_{K1} - m^2_{K1} + i m_{K1}\Gamma_{K1}} \tag{A22}$$

for the $K1(1270)$ resonance, where m_{sc} is the same scaling mass used in Sec. II. In terms of these combinations, the t-channel operators are given by

$$\hat{A}^t_{K^\star} = i\alpha^T_{K^\star}(E_{K^\star} f - \sigma \cdot \mathbf{p}_{K^\star} \sigma \cdot \xi),$$

$$\hat{B}^t_{K^\star} = -i\alpha^T_{K^\star}(E_{K^\star} \sigma \cdot \xi - f \sigma \cdot \mathbf{p}_{K^\star}),$$

$$\hat{C}^t_{K^\star} = i\alpha^V_{K^\star} f,$$

$$\hat{D}^t_{K^\star} = -i\alpha^V_{K^\star} \sigma \cdot \xi \tag{A23}$$

for the $K^\star(892)$ resonance, where

$$f = \epsilon \cdot \mathbf{p}_\gamma \times \mathbf{p}_K \tag{A24}$$

and

$$\xi = \epsilon \times (E_K \mathbf{p}_\gamma - E_\gamma \mathbf{p}_K), \tag{A25}$$

and

$$\hat{A}^t_{K1} = \alpha^T_{K1}[\epsilon \cdot \mathbf{p}_K \Omega(p_{K1}, p_\gamma) + \mathbf{p}_\gamma \cdot \mathbf{p}_K E_{K1} \sigma \cdot \epsilon],$$

$$\hat{B}^t_{K1} = \alpha^T_{K1}[\epsilon \cdot \mathbf{p}_K \Sigma(p_{K1}, p_\gamma) + \mathbf{p}_\gamma \cdot \mathbf{p}_K \sigma \cdot \mathbf{p}_{K1} \sigma \cdot \epsilon],$$

$$\hat{C}^t_{K1} = \alpha^V_{K1}[\mathbf{p}_\gamma \cdot \mathbf{p}_K \sigma \cdot \epsilon - \epsilon \cdot \mathbf{p}_K \sigma \cdot \mathbf{p}_\gamma],$$

$$\hat{D}^t_{K1} = \alpha^V_{K1} \epsilon \cdot \mathbf{p}_K E_\gamma \tag{A26}$$

for the $K1(1270)$ resonance.

[1] F. T. Hadjioannou, Phys. Rev. **125**, 1414 (1962); D. I. Julius, Nucl. Phys. **B21**, 173 (1970); P. Osland and A. K. Rey, Nuovo Cimento **32A**, 469 (1976); C. Lazard, R. J. Lombard, and Z. Maric, Nucl. Phys. **A271**, 317 (1976).

[2] J. M. Laget, Nucl. Phys. **A296**, 388 (1978).

[3] C. Lazard and Z. Maric, Nuovo Cimento Soc. Ital. Fis., A **16A**, 605 (1973); C. B. Dover and S. N. Yang, Phys. Lett. **50B**, 217 (1974); L. Tiator, A. K. Rej, and D. Drechsel, Nucl. Phys. **A333**, 343 (1980).

[4] H. Thom, Phys. Rev. **151**, 1322 (1966).

[5] F. M. Renard and Y. Renard, Nucl. Phys. **B25**, 490 (1971); Y. Renard, *ibid.* **B40**, 499 (1972).

[6] R. A. Adelseck, C. Bennhold, and L. E. Wright, Phys. Rev. C **32**, 1681 (1985).

[7] R. A. Adelseck and B. Saghai, Phys. Rev. C **42**, 108 (1990); Bijan Saghai and Frank Tabakin, *ibid.* **53**, 66 (1996).

[8] Robert A. Williams, Chueng-Ryon Ji, and Stephen R. Cotanch, Phys. Rev. C **46**, 1617 (1992).

[9] T. Mart, C. Bennhold, and C. E. Hyde-Wright, Phys. Rev. C **51**, R1074 (1995).

[10] M. K. Cheoun, B. S. Han, B. G. Yu, and Il-Tong Cheon, Phys. Rev. C **54**, 1811 (1996).

[11] J. C. David, C. Fayard, G. H. Lamot, and B. Saghai, Phys. Rev. C **53**, 2613 (1996).

[12] T. Mizutani, C. Fayard, G.-H. Lamot, and B. Saghai, Phys. Rev. C **58**, 75 (1998).

[13] S. Janssen, J. Ryckebusch, W. Van Nespen, D. Debruyne, and T. Van Cauteren, Eur. Phys. J. A **11**, 105 (2001); S. Janssen, J. Ryckebusch, D. Debruyne, and T. Van Cauteren, Phys. Rev. C **65**, 015201 (2002); S. Janssen, D. G. Ireland, and J. Ryckebusch, Phys. Lett. B **562**, 51 (2003); S. Janssen, J. Ryckebusch, and T. Van Cauteren, Phys. Rev. C **67**, 052201 (2003).

[14] F. M. Renard and Y. Renard, Nucl. Phys. **B1**, 389 (1967); Phys. Lett. **24B**, 159 (1967).

[15] R. A. Adelseck and L. E. Wright, Phys. Rev. C **39**, 580 (1989).

[16] Xiaodong Li and L. E. Wright, J. Phys. G **17**, 1127 (1991).

[17] H. Yamamura, K. Miyagawa, T. Mart, C. Bennhold, H. Haberzettl, and W. Glockle, Phys. Rev. C **61**, 014001-1 (1999).
[18] T. Mart, L. Tiator, D. Drechsel, and C. Bennhold, Nucl. Phys. **A640**, 235 (1998).
[19] CNS Data Analysis Center website; John S. Hyslop, Richard A. Arndt, L. David Roper, and Ron L. Workman, Phys. Rev. D **46**, 961 (1992).
[20] C. Caso *et al.*, Eur. Phys. J. C **3**, 1 (1998).
[21] David Faiman, Nucl. Phys. **B32**, 573 (1971); D. Faiman and D. E. Plane, *ibid.* **B50**, 379 (1972); D. Faiman, *ibid.* **B115**, 478 (1976).
[22] A. J. G. Hey, P. J. Litchfield, and R. J. Cashmore, Nucl. Phys. **B95**, 516 (1975).
[23] M. Benmerrouche, R. M. Davidson, and Nimai C. Mukhopadhyay, Phys. Rev. C **39**, 2339 (1989).
[24] V. Pascalutsa, Phys. Rev. D **58**, 096002 (1998); Nucl. Phys. **A680**, 76C (2001); Phys. Lett. B **503**, 85 (2001).
[25] T. Feuster and U. Mosel, Phys. Rev. C **59**, 460 (1999).
[26] S. Coleman and S. L. Glashow, Phys. Rev. Lett. **6**, 423 (1961).
[27] H. Pilkuhn, *The Interaction of Hadrons* (North-Holland, Amsterdam, 1967).
[28] J. J. de Swart, Rev. Mod. Phys. **35**, 916 (1963).
[29] O. Dumbrajs *et al.*, Nucl. Phys. **B216**, 277 (1983).